Mathematical model of calcium exchange during hemodialysis using a citrate containing dialysate

Julien Aniort, Laurent Chupin, Nicolae Cindea

Mathematical model of calcium exchange during hemodialysis using a citrate containing dialysate

Julien Aniort*, Laurent Chupin†, Nicolae Cîndea‡

January 12, 2017

Abstract

In this paper we propose a mathematical model for the calcium exchange during hemodialysis. This model combines a first part describing the flows of two fluids, blood and dialysate, in a dialyser fiber to a second part which tackle the chemical reactions between several chemical species present in these fluids. The model governing the fluid flows is obtained by asymptotic analysis and takes into account the anisotropy of the fibers forming a dialyzer. We complete this partial differential equations system by standard boundary conditions, the specificity of our study being that we optimize the values of input and output pressures such that the blood and dialysate flow rates match the values measured on clinical dialyzers. In order to to highlight the differences in the flow, several rheologies for blood are proposed. The fluid velocity field drives the convective part in the reaction–diffusion system, modelling the exchange of five chemical species present in blood and dialysate. Finally, several numerical experiments illustrate this model emphasizing the calcium balance for citrate containing dialysates.

1 Introduction

Renal replacement therapy with hemodialysis is used in patient with end stage renal disease to remove uremic toxins and restore blood electrolytes composition [16]. End stage renal disease leads to mineral metabolism changes, bone disorders and cardiovascular calcifications [13]. All are related with high mortality rate in chronic hemodialysis patients. Balance between calcium intake and loss during hemodialysis treatment affects these abnormalities. Therefore, it is essential to be able to predict calcium exchange with hemodialysis. Heparin is the most routinely used anticoagulant for the prevention of extracorporeal circulation clotting during hemodialysis sessions. However, heparin exposes the patient to the risk of bleeding complications and heparin induced thrombocytopenia [6]. To avoid these complications, regional anticoagulation of blood circuit can be realized using a citrate containing dialysate [20]. Citrate is a potent calcium chelator and the anticoagulant properties of citrate dialysate are believed to be caused by the decrease in free calcium concentration of the blood. However, this hypothesis has not yet been confirmed since it is not possible to measure the free calcium concentration distribution into the dialyzer. In the present study we propose to use a modeling of fluid and solutes transport to predict the amount of calcium exchanged between blood and dialysate and the distribution of free calcium concentration into the dialyzer.

*Service de nephrologie, dialyse et tranplantation rénale. Centre Hospitalier Universitaire Gabriel Montpied, Clermont-Ferrand (janiort@chu-clermontferrand.fr)

†Université Clermont Auvergne, Laboratoire de Mathématiques Blaise Pascal CNRS-UMR 6620, Campus des Cézeaux, F-63177 Aubière cedex, France (laurent.chupin@math.univ-bpclermont.fr)

‡Université Clermont Auvergne, Laboratoire de Mathématiques Blaise Pascal CNRS-UMR 6620, Campus des Cézeaux, F-63177 Aubière cedex, France (nicolae.cindea@math.univ-bpclermont.fr)

The one-dimensional theory of solute transport in dialyzer provides a simplified description of solute flows in blood and dialysate channels, assuming that the average concentration of the solute in any cross-section of the channel is equal to the concentration of the solute at the surface of the membrane. Transport in membrane is modeled according to the Kedem and Katchalsky equation [18] with Villarroel correction [33] used to account for convection-diffusion interaction. One-dimensional axially-dependent models based on ordinary differential equations have provided much insight into the dynamics of fluid and solutes within and around the hollow fibers. However, they have several limitations. Notably, the assumption of homogeneous solute concentration in the cross-section of the channels does not allow computing the distribution of concentration into the dialyser. Resolution of partial differential equations using finite elements method eliminates the need for most of the simplifying assumptions and potentially generates more accurate results. Few studies about calcium flux modeling into the dialyzer have been conducted. Gotch et al [12] proposes to use the concept of dialysance in a way analogous to urea for calculating the calcium flux through the dialyser. However, there is no evidence that calcium dialysance is independent of the concentration of calcium and other solutes reacting with calcium. Moreover, calcium binding to albumin and diffusible calcium complexes are not taken into account [12]. Thijssen et al [31] completed Gotch's model adding the calculation of the concentrations of complexes derived from calcium, citrate and albumin at equilibrium. But it is only Huang et al [17] who considered the interactions between diffusion, convection and chemical reaction within the dialyzer. Their model is based on one-dimensional theory. A step of calculating concentrations after the equilibrium of reaction is reached was added to the algorithm making it possible to calculate the concentrations within the dialyzer. However, this model as other one-dimensional theory models does not give the concentration gradient of calcium within the blood compartment.

In the present study we propose a modelling of flows and concentrations, notably of calcium ions, in a dialyser using citrate containing dialysate. The blood is modelled as a Newtonian or, as a well, as a non-Newtonian fluid, the dialysate fluid is described as a Newtonian fluid and the flow in the membrane is governed by Darcy's equation. The main novelty with respect to the existing literature [8, 7, 10] on the flow models is in choice of the boundary conditions which drive the flow. We only impose the pressures at the inlet and outlet of a hollow fiber for the blood and dialysate respectively. Since these pressures at the level of a fiber are not generally available, in practice we compute the pressure boundary data using an optimization algorithm providing a set of pressures such that the resulting solution fits the blood and dialysate global flow rates at the level of the hemodialysis machine. This procedure allows us to consider several different rheologies for the non-Newtonian fluid governing the blood flow and to obtain a velocity field of the fluids in a dialyzer such that the blood flow rate and the dialysate flow rate available on every standard hemodialysis machine are fitted by the model.

The velocity field computed by solving the fluid model enters in the convective part of the convection-diffusion-reaction system describing the interaction of five different chemical species presented in blood and in dialysate. Since the albumin, which is one of the considered species, exerts an oncotic pressure in the blood, the model describing the evolution of the velocity of the fluids should take into account this supplementary pressure. In this case the fluid model is strongly coupled to the convection-diffusion-reaction system and that makes the whole system difficult to handle from both theoretical and numerical point of view. In order to simplify the model, the assumption usually made in the literature [19, 21] is that the oncotic pressure depends linearly to the longitudinal variable in a fiber and is radially invariant. This is equivalent to assume that the concentration of albumin, or in general of proteins, is monotonic in one hollow fiber with respect to the longitudinal variable. For the present study we adopt this hypothesis, even if the numerical simulations show that for pressure data corresponding to clinical situations the concentration of albumin is non-monotonic in both situations if the osmotic pressure is took into account by the model or not. The study of the coupled model fluid-convection-reaction-diffusion will make the object of a future study.

The plan of this paper is as follows. In Section 2 we schematically describe the geometry of a dialyzer which allow us to introduce some notations. Section 3 is devoted to the study of the hydrodynamic flow

in a fiber of the dialyzer and follows the ideas in [10]. The conservation equations are introduced in the subsection 3.1 to describe the fluid velocity and the fluid pressure in the blood, in the membrane and into the dialysate. Conditions at the interfaces are provided to couple all the unknowns. After a step of nondimensionalization we simplify the model in the subsection 3.3 taking into account the low ratio between the width and the length of a fiber. Several rheological models for the blood are described in the subsection 3.4. The results obtained for different rheologies are compared in the subsection 3.5 after having described the variational formulation and the numerical scheme employed to approach the solution of the system. In the Section 4, we describe the convection-reaction-diffusion equations used to monitor the concentration of different products in the dialyzer. Again the model is reduced using a nondimensionalization and asymptotic analysis. Section 5 illustrate the model introduced in the previous section by numerical experiments and Section 6 gives some conclusions and perspectives for this work.

2 Simplified geometry of a dialyser

The aim of this section is to present the geometrical model which is considered in this paper in order to propose a mathematical model for a dialyser.

A dialyser module consists of an array of a large number N of equispaced parallel hollow fibers. Each fiber is composed of three parts: a central channel, a permeable membrane surrounding this channel, and an outer channel delimited by an ideal no-flux boundary confining the permeate flow. The blood flow is confined in the inner channel while the dialysate flows in the outer channel and in the opposite direction. We may focus on studying the flow in a single cell whose geometry is equivalent to the geometry of a pipe (see, for instance, [7, 8, 10] and the references therein). We assume that in each hollow fiber the flows are radially symmetric and, hence, it is natural to work using the cylindrical coordinates. The problem can be reduced to a two-dimensional one in a domain Ω defined by

$$\Omega = \Big\{(x,r) \in \mathbb{R}^2 \quad ; \quad 0 < x < L \quad \text{and} \quad 0 < r < R\Big\},$$

where L is the length of the fiber, and where R is its radius. This domain is naturally separated into three sub-domains corresponding to the blood domain Ω_b, the membrane domain Ω_m and the dialysate domain Ω_d, whose sizes are described by the positive real numbers R_1 and R_2, respectively:

$$\begin{aligned}
\Omega_b &= \Big\{(x,r) \in \Omega \quad ; \quad 0 < r < R_1\Big\},\\
\Omega_m &= \Big\{(x,r) \in \Omega \quad ; \quad R_1 < r < R_2\Big\},\\
\Omega_d &= \Big\{(x,r) \in \Omega \quad ; \quad R_2 < r < R\Big\}.
\end{aligned}$$

The interfaces between these domains are denoted Γ_{bm} and Γ_{md} and are defined by

$$\begin{aligned}
\Gamma_{bm} &= \Big\{(x,r) \in \Omega \quad ; \quad r = R_1\Big\},\\
\Gamma_{md} &= \Big\{(x,r) \in \Omega \quad ; \quad r = R_2\Big\}.
\end{aligned}$$

Finally, we describe the boundary of the domain as several *natural* sub-boundaries. Therefore, the left side of the rectangle Ω is composed by the union of three segments: $\Gamma_{l,b}$, corresponding to the left side of the blood channel, $\Gamma_{l,m}$, corresponding to the left boundary of the membrane, and $\Gamma_{l,d}$ which corresponds to the left side of the dialysate outlet, respectively. The right side of Ω is, symmetrically, formed by three segments $\Gamma_{r,b}$, $\Gamma_{r,m}$ and $\Gamma_{r,d}$. We recall that the blood flows from left to right and the dialysate flows in the opposite direction. All these boundaries are illustrated in Figure 1 and precisely described by the

following equations:

$$\Gamma_b = \Big\{(x,0) \in \mathbb{R}^2 \ ; \ x \in (0,L)\Big\}, \qquad \Gamma_d = \Big\{(x,R) \in \mathbb{R}^2 \ ; \ x \in (0,L)\Big\} \tag{1}$$

$$\Gamma_{bm} = \big\{(x,R_1) \in \mathbb{R}^2 \ ; \ x \in (0,L)\big\}, \qquad \Gamma_{md} = \big\{(x,R_2) \in \mathbb{R}^2 \ ; \ x \in (0,L)\big\}, \tag{2}$$

$$\Gamma_{\ell,b} = \big\{(0,r) \in \mathbb{R}^2 \ ; \ r \in (0,R_1)\big\}, \qquad \Gamma_{r,b} = \big\{(L,r) \in \mathbb{R}^2 \ ; \ r \in (0,R_1)\big\}, \tag{3}$$

$$\Gamma_{\ell,m} = \big\{(0,r) \in \mathbb{R}^2 \ ; \ r \in (R_1,R_2)\big\}, \qquad \Gamma_{r,m} = \big\{(L,r) \in \mathbb{R}^2 \ ; \ r \in (R_1,R_2)\big\}, \tag{4}$$

$$\Gamma_{\ell,d} = \big\{(0,r) \in \mathbb{R}^2 \ ; \ r \in (R_2,R)\big\}, \qquad \Gamma_{r,d} = \big\{(L,r) \in \mathbb{R}^2 \ ; \ r \in (R_2,R)\big\}. \tag{5}$$

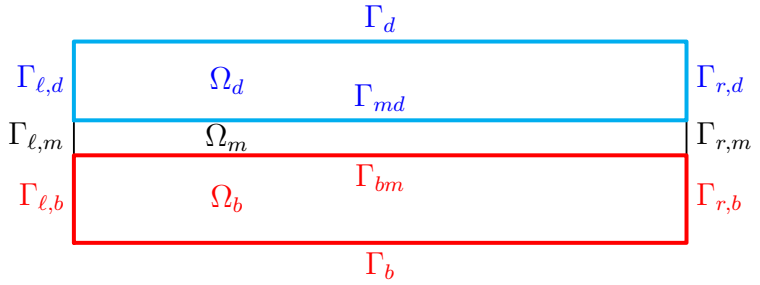

Figure 1: Geometry and boundaries of a fiber.

In fact, due to the large difference between the two lengths L and R (typically $L = 23\,\text{cm}$ and $R = 0.23\,\text{mm}$), it will be interesting to work in a re-scaled domain. We will take into account this anisotropy in Section 3. Finally, the schematic simplification of the geometry of the dialyser is described in Figure 2.

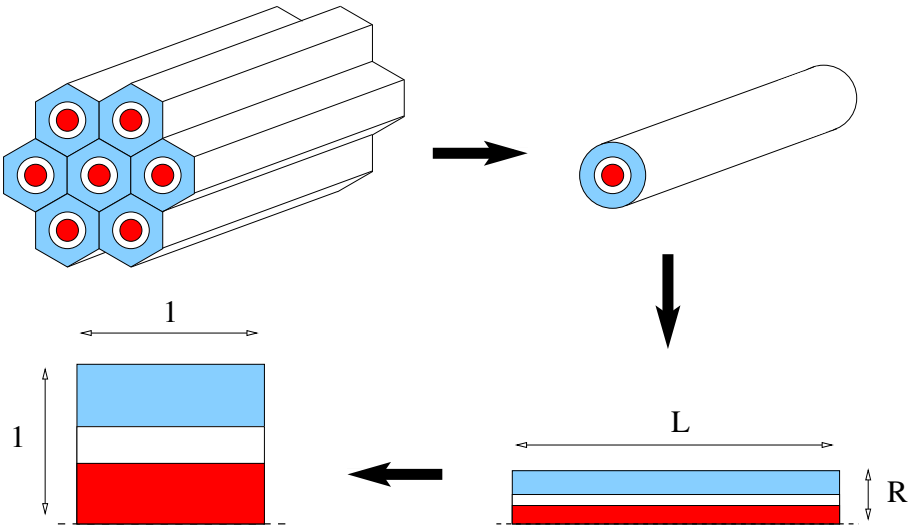

Figure 2: The reduction process of the initial problem on a complex physical geometry to a problem in a square: first, considering only one fiber; second, using cylindrical coordinates; third, scaling the domain.

3 Modelling of flow in a fiber

3.1 Governing equations

The flow in a fiber is characterized by its velocity field and its pressure. The model described here is based on the physical conservation of mass and momentum, and it is first introduced on each sub-domain

corresponding to the blood domain, to the membrane and then to the dialysate domain, respectively. The notations for each sub-domain are outlined in Table 1. Some interface conditions are next introduced between these connected domains.

Domain	Pressure	Velocity	Model
Blood: Ω_b	p_b	(v_x, v_r)	Non-Newtonian fluid
Membrane: Ω_m	p_m	(u_x, u_r)	Darcy's equation
Dialysate: Ω_d	p_d	(w_x, w_r)	Newtonian fluid

Table 1: Notation for pressure, velocity fields and the physical model corresponding to the three sub-domains of domain Ω.

3.1.1 Blood flow

The blood is modelled either as a Newtonian fluid, either as a quasi-Newtonian fluid. The equations satisfied by the velocity field (v_x, v_r) and the pressure p_b correspond to the mass and the momentum conservation laws. These equations are valid for $(x, r) \in \Omega_b$ and for any time $t > 0$:

$$\begin{cases} \rho\Big(\partial_t v_x + v_x\partial_x v_x + \dfrac{1}{r}v_r\partial_r(rv_x)\Big) = -\partial_x p_b + 2\mu\,\partial_x\Big(G(\dot\gamma)\,\partial_x v_x\Big) + \dfrac{\mu}{r}\partial_r\Big(r\,G(\dot\gamma)\,(\partial_r v_x + \partial_x v_r)\Big) - \partial_x p_{\mathrm{o}}, \\ \rho\Big(\partial_t v_r + v_x\partial_x v_r + \dfrac{1}{r}v_r\partial_r(rv_r)\Big) = -\partial_r p_b + 2\dfrac{\mu}{r}\partial_r\Big(r\,G(\dot\gamma)\,\partial_r v_r\Big) + \mu\,\partial_x\Big(G(\dot\gamma)\,(\partial_r v_x + \partial_x v_r)\Big) - \partial_r p_{\mathrm{o}}, \\ \partial_x v_x + \dfrac{1}{r}\partial_r(rv_r) = 0. \end{cases}$$

The constant blood density is denoted by $\rho = 10^3$ kg.m^{-3}. We will consider some different rheology models for the blood. The viscosity of the blood will be given by $\mu\,G(\dot\gamma)$, where G is a function of the shear rate:

$$\dot\gamma = \sqrt{|\partial_x v_x|^2 + |\partial_r v_r|^2 + \Big|\frac{v_r}{r}\Big|^2 + \frac{1}{2}|\partial_r v_x + \partial_x v_r|^2}.$$

Here and henceforth, μ denotes the reference viscosity and is equal to the viscosity of the water ($\mu = 10^{-3}$ Pa.s). Some examples of functions G will be given in subsection 3.4.

The oncotic pressure p_{o} depends on the concentration of suspended proteins in the blood. In this study we assume that the oncotic pressure is constant with respect to the radial variable r and depends linearly to the spatial variable x. This assumption reflects the fact that the suspension of proteins in blood becomes more concentrated as it moves through the hollow fiber (see, for instance, [19, Chapter 20]) and translates into the fact that $\partial_x p_{\mathrm{o}}$ is constant and $\partial_r p_{\mathrm{o}} = 0$. The precise values of the oncotic pressure at blood inlet and at the blood outlet, respectively, are computed as in [21, Equation (20)].

3.1.2 Membrane flow

In the porous membrane, the governing equations are the continuity equation (corresponding to the free-divergence of the flux) coupled with Darcy's law (corresponding to the fact that the flux is proportional to the gradient of the pressure p_m). For $(x, r) \in \Omega_m$, these two equations give:

$$\partial_x^2 p_m + \frac{1}{r}\partial_r(r\partial_r p_m) = 0.$$

The velocity field in the membrane is denoted (u_x, u_r) and is obtained from the following relations

$$\begin{cases} u_x = -\dfrac{K}{\mu}\partial_x p_m, \\ u_r = -\dfrac{K}{\mu}\partial_r p_m, \end{cases}$$

the coefficient K corresponding to the permeability of the membrane.

3.1.3 Dialysate flow

The dialysate is supposed to be a Newtonian fluid with the same constant density as the blood, and with a viscosity equal to the reference viscosity μ. Navier-Stokes equations on the velocity (w_x, w_r) and the pressure p_d read, for $(x, r) \in \Omega_d$ and for any time $t > 0$:

$$\begin{cases} \rho\Big(\partial_t w_x + w_x\partial_x w_x + \dfrac{1}{r}w_r\partial_r(rw_x)\Big) = -\partial_x p_d + \mu\partial_x^2 w_x + \dfrac{\mu}{r}\partial_r(r\partial_r w_x), \\ \rho\Big(\partial_t w_r + w_x\partial_x w_r + \dfrac{1}{r}w_r\partial_r(rw_r)\Big) = -\partial_r p_d + \dfrac{\mu}{r}\partial_r(r\partial_r w_r) + \mu\partial_x^2 w_r, \\ \partial_x w_x + \dfrac{1}{r}\partial_r(rw_r) = 0. \end{cases}$$

3.1.4 Interface blood-membrane

The conditions imposed at the interface blood/membrane Γ_{bm} correspond to the continuity of the flux, Saffman's condition (see for instance [10]) for the slip velocity, and the continuity of the pressure, respectively. For every $(x, r) \in \Gamma_{bm}$ these conditions write as follows:

$$\begin{cases} v_r = -\dfrac{K}{\mu}\partial_r p_m, \\ -\partial_r v_x = \dfrac{\alpha_{\mathrm{BJ}}}{\sqrt{K}}v_x, \\ p_m = p_b, \end{cases}$$

where the coefficient α_{BJ} is the Beavers-Joseph constant (measured slip coefficient only depends on porous media properties) relative to the channel porous wall.

3.1.5 Interface membrane-dialysate

The conditions on the interface membrane/dialysate Γ_{md} are similar to the conditions on the interface blood/membrane, with the difference that the Beavers-Joseph constant appearing here is different to the one appearing for Γ_{bm}. More precisely, for every $(x, r) \in \Gamma_{md}$ we have:

$$\begin{cases} w_r = -\dfrac{K}{\mu}\partial_r p_m, \\ \partial_r w_x = \dfrac{\beta_{\mathrm{BJ}}}{\sqrt{K}}w_x, \\ p_m = p_d, \end{cases}$$

where the coefficient β_{BJ} is another Beavers-Joseph constant relative to the channel porous wall.

3.1.6 Boundary conditions for the flow

The boundary of the domain is composed of the lateral boundaries described by $x = 0$ and $x = L$, by the "exterior" boundary $r = R$ and by the symmetry axis $r = 0$. The physical conditions on these boundaries are given by:

$p_b = p_{b,\text{in}}$ on $\Gamma_{\ell,b}$,	$p_b = p_{b,\text{out}}$ on $\Gamma_{r,b}$	for the blood pressure;
$p_d = p_{d,\text{in}}$ on $\Gamma_{r,d}$,	$p_d = p_{d,\text{out}}$ on $\Gamma_{\ell,d}$	for the dialysate pressure;
$w_r = 0$ on Γ_d,	$\partial_r w_x = 0$ on Γ_d	top boundary;
$\partial_r v_x = 0$ on Γ_b		symmetry axis.

The first boundary conditions correspond to the imposed pressures both on the blood and on the dialysate. An assumption usually made in the literature is that these pressures satisfy $p_{b,\text{in}} > p_{b,\text{out}} > p_{d,\text{in}} > p_{d,\text{out}}$ (see [8, 7] or [10, Table 3] for typical values of these pressures).

In order to have a well posed system, we complete these boundary conditions by considering some homogeneous Neumann boundary conditions on the other parts of the boundary of Ω:

$$\begin{aligned}
&\partial_r p_b = 0 && \text{on } \Gamma_b,\\
&\partial_r p_d = 0 && \text{on } \Gamma_d,\\
&\partial_x v_x = \partial_x v_r = 0 && \text{on } \Gamma_{\ell,b} \cup \Gamma_{r,b},\\
&\partial_x w_x = \partial_x w_r = 0 && \text{on } \Gamma_{\ell,d} \cup \Gamma_{r,d},\\
&\partial_x p_m = 0 && \text{on } \Gamma_{\ell,m} \cup \Gamma_{r,m}.
\end{aligned}$$

All these Neumann conditions appear naturally in the weaker variational formulation described in Appendix B and allow us to cancel some boundary integrals. From a physical point of view, the conditions on Γ_b and Γ_d state that the pressures in the blood and in the dialysate, respectively, are constant radially near the both boundaries. The conditions on the lateral boundaries impose the fact that the velocity and the pressure are locally constant in the longitudinal direction at both extremities of the fiber.

3.2 Scaling procedure

In this section we replace the physical quantities appearing in the model by dimensionless quantities and we rewrite in consequence the corresponding equations. Firstly, we setup the reference density ρ and the reference viscosity μ to the density and viscosity of water:

$$\rho = 10^3 \text{ kg.m}^{-3}, \qquad \mu = 10^{-3} \text{ Pa.s.}$$

In Table 2 we gather two sets of parameters describing the geometry and the permeability of two typical dialyzers. The first set of parameters describe the dialyzer machine in [8] and the second one lists the product specifications of a universal dialyzer APS-18U ®. Table 3 list typical values of blood and dialysate injection/output pressures in a hollow fiber [8, 10].

3.2.1 Reference quantities

Some characteristic sizes appear naturally in the formulation of the problem: two lengths L and R, and four pressures: $p_{b,\text{in}}$, $p_{b,\text{out}}$, $p_{d,\text{in}}$ and $p_{d,\text{out}}$. In practice, we will use the difference

$$P = p_{b,\text{in}} - p_{b,\text{out}}$$

as a reference pressure. Using this reference pressure, the reference viscosity μ and the two characteristic lengths R and L, it is possible to define a reference velocity:

$$V = \frac{PR^2}{\mu L}.$$

In fact, it is also possible to introduce another reference pressure using the difference $p_{d,\text{in}} - p_{d,\text{out}}$. The corresponding velocity, denoted W, is given by $W = \mathcal{P}_1 V$ where

$$\mathcal{P}_1 = \frac{p_{d,\text{in}} - p_{d,\text{out}}}{P}. \tag{6}$$

We will also use another quantity to take into account all the pressures imposed on the boundaries of the domain:

$$\mathcal{P}_2 = \frac{p_{b,\text{out}} - p_{d,\text{in}}}{P}. \tag{7}$$

We note that the first velocity V will be used for the nondimensionalization of the blood velocity whereas the second velocity W will be used in order to nondimensionalize the dialysate velocity. Finally, we introduce the reference time by

$$T = \frac{L}{V}.$$

3.2.2 Dimensionless numbers

The following dimensionless numbers can be defined:

$$\varepsilon = \frac{R}{L}, \quad \mathcal{R}e = \frac{\rho R V}{\mu}, \quad \mathcal{D}a = \frac{K}{R^2}, \quad B_b = \frac{\alpha_{\text{BJ}}}{\sqrt{\mathcal{D}a}}, \quad B_d = \frac{\beta_{\text{BJ}}}{\sqrt{\mathcal{D}a}}.$$

These numbers will be used to write the complete system of partial differential equations in a dimensionless form. The first parameter describes the ratio between the two lengths previously introduced. In practice, the number ε is much smaller than 1 and the Reynolds number $\mathcal{R}e$ will be of order 1. The number $\mathcal{D}a$ corresponds to the Darcy number and the quotient $\mathcal{D}a/\varepsilon^2$ is of order 1. It is more difficult to evaluate the Beaver-Joseph coefficients α_{BJ} and β_{BJ}. These parameters depend on the properties of the porous material as well as the material specific surface conditions. In [26] and more recently in [4], the authors take $\beta_{\text{BJ}} = 1$. We addopt this hypothesis for the present work. In this case, the product εB_d is of order 1, that corresponds to the Remark 3 in [10, page 1918]. Following [10] again, the boundary condition on the interface blood-membrane must slip into play. They propose to use a coefficient α_{BJ} such that the parameter B_b is of order 1 with respect to ε (more precisely, we use the value given as example in [10, Table 7]). This difference between the two Beavers-Joseph's coefficients is related to the fact that, contrary to dialysate, the blood do not adhere at the membrane surface.

Name	Notation	Set A		Set B	
Length	L	2.3×10^{-1}	m	3.3×10^{-1}	m
Total radius	R	2.3×10^{-4}	m	2.1×10^{-4}	m
Blood radius	R_1	10^{-4}	m	10^{-4}	m
Membrane radius	R_2	1.4×10^{-4}	m	1.45×10^{-4}	m
Permeability	K	2.4×10^{-18}	m^2	1.21×10^{-17}	m^2
Number of fibers	N	10^4		10^4	

Table 2: Two set of values describing two different dialyzers

We list below an example of non-dimensional numbers corresponding to Set A of data in Table 2 (see [10, Remark 3] for the typical values of Beavers-Joseph number B_d which is assumed to be large, typically of order of $1/\varepsilon$):

$$\varepsilon = 10^{-3}, \quad \mathcal{R}e = 124.836, \quad \mathcal{D}a = 4.537 \times 10^{-11}, \quad B_b = 2.5, \quad B_d = 7.3 \times 10^3.$$

Name	Notation	Value
Blood injection pressure	$p_{b,\text{in}}$	16×10^3 Pa
Blood output pressure	$p_{b,\text{out}}$	11×10^3 Pa
Dialysate injection pressure	$p_{d,\text{in}}$	1×10^3 Pa
Dialysate output pressure	$p_{d,\text{out}}$	0.1×10^3 Pa

Table 3: Typical values for pressure data (see, for instance, [10, Table 3]) corresponding to a dialyzer described by Set A in Table 2.

We use the following scaling for the different variables (the star notation $\star$ corresponding to variables without dimension):

$$x = L\,x^\star, \quad r = R\,r^\star, \quad t = T\,t^\star, \quad p_a = p_{b,\text{out}} + P\,p_a^\star, \quad \text{for } a \in \{b, m, d, o\},$$
$$v_x = V\,v_x^\star, \quad v_r = \varepsilon V\,v_r^\star, \quad u_x = W\,u_x^\star, \quad u_r = \varepsilon W\,u_r^\star \quad w_x = W\,w_x^\star, \quad w_r = \varepsilon W\,w_r^\star.$$

Note that, since the pressure is defined up to an additive constant, we choose $p_{b,\text{out}}$ as a reference pressure. It is then possible to rewrite all the equations describing the flow under a dimensionless form. For clarity, these equations are postponed in the Appendix A. We only indicate here the domains in which the equations hold since this notation will be re-used in the following sections.

Firstly, the domain Ω becomes, after the scaling, the unit square ω:

$$\omega = \Big\{(x^\star, r^\star) \in \mathbb{R}^2 \quad ; \quad 0 < x^\star < 1 \quad \text{and} \quad 0 < r^\star < 1\Big\}.$$

Similarly to domain Ω, the rescaled domain ω is composed by three subdomains:

$$\omega_b = \Big\{(x^\star, r^\star) \in \omega \quad ; \quad 0 < r^\star < \frac{R_1}{R}\Big\},$$
$$\omega_m = \Big\{(x^\star, r^\star) \in \omega \quad ; \quad \frac{R_1}{R} < r^\star < \frac{R_2}{R}\Big\},$$
$$\omega_d = \Big\{(x^\star, r^\star) \in \omega \quad ; \quad \frac{R_2}{R} < r^\star < 1\Big\}$$

and its boundary is formed by the following segments:

$$\gamma_b = \Big\{(x^\star, 0) \in \mathbb{R}^2 \quad ; \quad x^\star \in (0,1)\Big\}, \qquad \gamma_d = \Big\{(x^\star, 1) \in \mathbb{R}^2 \quad ; \quad x^\star \in (0,1)\Big\},$$
$$\gamma_{bm} = \left\{\left(x^\star, \frac{R_1}{R}\right) \in \mathbb{R}^2 \quad ; \quad x^\star \in (0,1)\right\}, \qquad \gamma_{md} = \left\{\left(x^\star, \frac{R_2}{R}\right) \in \mathbb{R}^2 \quad ; \quad x^\star \in (0,1)\right\},$$
$$\gamma_{\ell,b} = \left\{(0, r^\star) \in \mathbb{R}^2 \quad ; \quad r^\star \in \left(0, \frac{R_1}{R}\right)\right\}, \qquad \gamma_{r,b} = \left\{(1, r^\star) \in \mathbb{R}^2 \quad ; \quad r^\star \in \left(0, \frac{R_1}{R}\right)\right\},$$
$$\gamma_{\ell,m} = \left\{(0, r^\star) \in \mathbb{R}^2 \quad ; \quad r^\star \in \left(\frac{R_1}{R}, \frac{R_2}{R}\right)\right\}, \quad \gamma_{r,m} = \left\{(1, r^\star) \in \mathbb{R}^2 \quad ; \quad r^\star \in \left(\frac{R_1}{R}, \frac{R_2}{R}\right)\right\},$$
$$\gamma_{\ell,d} = \left\{(0, r^\star) \in \mathbb{R}^2 \quad ; \quad r^\star \in \left(\frac{R_2}{R}, 1\right)\right\}, \qquad \gamma_{r,d} = \left\{(1, r^\star) \in \mathbb{R}^2 \quad ; \quad r^\star \in \left(\frac{R_2}{R}, 1\right)\right\}.$$

To fix the notation, we graphically represent in Figure 3 the domain ω with its subdomains and their boundaries.

3.3 Considerations on the geometric anisotropy of a fiber

During the scaling process, we have introduced a dimensionless number ε which is very small with respect to 1. To get a simpler system we will keep only the main order terms with respect to ε, taking into account

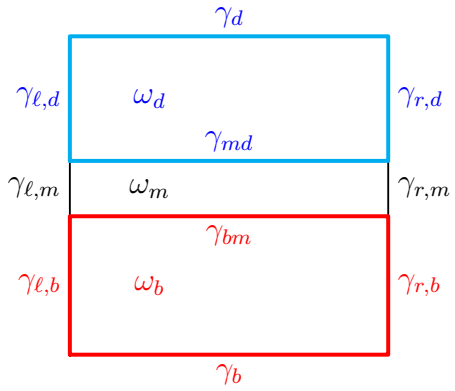

Figure 3: Domain ω, its subdomains and their boundaries.

that

$$\widetilde{\mathcal{D}a} = \frac{\mathcal{D}a}{\varepsilon^2} = \mathcal{O}(1) \quad \text{and} \quad B_d = \mathcal{O}\Big(\frac{1}{\varepsilon}\Big),$$

all the other parameters being of order 1.
Taking into account this anisotropy ($\varepsilon \ll 1$), we can formally simplify the set of equations describing the flow. More precisely, the equations obtained in the Appendix A can be approximated by the equations described below.

For every $(x^\star, r^\star) \in \omega_b$ the simplified blood flow is governed by the following equation

$$\begin{cases} 0 = -\partial_{x^\star} p_b^\star + \dfrac{1}{r^\star}\partial_{r^\star}\Big(r^\star\, \widetilde{G}(\dot\gamma)\, \partial_{r^\star} v_x^\star\Big) - \partial_{x^\star} p_{\mathrm{o}}^\star, & \text{(8a)} \\ 0 = -\partial_{r^\star} p_b^\star, & \text{(8b)} \\ \partial_{x^\star} v_x^\star + \dfrac{1}{r^\star}\partial_{r^\star}(r^\star v_r^\star) = 0, & \text{(8c)} \end{cases}$$

where the shear rate reduces to $\dot\gamma = \dfrac{1}{\varepsilon\sqrt{2}}|\partial_{r^\star} v_x^\star|$, and the function $\widetilde{G}$ is defined from the viscosity function G as follows

$$\widetilde{G}(X) = G\Big(\frac{\varepsilon^2 P}{\mu} X\Big). \tag{9}$$

The pressure and the velocities into the membrane domain ω_m satisfy

$$\begin{cases} \partial_{r^\star}(r^\star \partial_{r^\star} p_m^\star) = 0, & \text{(10a)} \\ u_x^\star = 0, & \text{(10b)} \\ u_r^\star = -\dfrac{\widetilde{\mathcal{D}a}}{\mathcal{P}_1}\partial_{r^\star} p_m^\star, & \text{(10c)} \end{cases}$$

and the dialysate flow is given by the solution of the following equation:

$$\begin{cases} 0 = -\partial_{x^\star} p_d^\star + \dfrac{\mathcal{P}_1}{r^\star}\partial_{r^\star}(r^\star \partial_{r^\star} w_x^\star), & \text{(11a)} \\ 0 = -\partial_{r^\star} p_d^\star, & \text{(11b)} \\ \partial_{x^\star} w_x^\star + \dfrac{1}{r^\star}\partial_{r^\star}(r^\star w_r^\star) = 0. & \text{(11c)} \end{cases}$$

Finally, the simplified conditions at the interfaces blood/membrane, membrane/dialysate and at the exterior boundaries became:

✓ interface blood/membrane (on γ_{bm}):

$$\begin{cases} v_r^\star = -\widetilde{\mathcal{D}a}\,\partial_{r^\star} p_m^\star, & \text{(12a)} \\ -\partial_{r^\star} v_x^\star = B_b v_x^\star, & \text{(12b)} \\ p_m^\star = p_b^\star. & \text{(12c)} \end{cases}$$

✓ interface membrane/dialysate (on γ_{md}):

$$\begin{cases} w_r^\star = -\dfrac{\widetilde{\mathcal{D}a}}{\mathcal{P}_1}\partial_{r^\star} p_m^\star, & \text{(13a)} \\ w_x^\star = 0, & \text{(13b)} \\ p_m^\star = p_d^\star. & \text{(13c)} \end{cases}$$

✓ exterior boundary conditions:

$$\begin{cases} p_b^\star|_{\gamma_{\ell,b}} = 1, \qquad p_b^\star|_{\gamma_{r,b}} = 0, & \text{(14a)} \\ p_d^\star|_{\gamma_{r,d}} = -\mathcal{P}_2, \qquad p_d^\star|_{\gamma_{\ell,d}} = -\mathcal{P}_2 - \mathcal{P}_1, & \text{(14b)} \\ w_r^\star|_{\gamma_d} = \partial_{r^\star} w_x^\star|_{\gamma_d} = 0, & \text{(14c)} \\ \partial_{r^\star} v_x^\star|_{\gamma_b} = 0. & \text{(14d)} \end{cases}$$

Remark 3.1 *From this system, it is not difficult to determine the membrane pressure $p_m^\star$. This pressure satisfies the ordinary differential equation* (10a) *within the two boundary Dirichlet conditions* (12c) *and* (13c)*. We deduce the following expression of $p_m^\star$ with respect to the pressures $p_b^\star$ and $p_d^\star$: for $(x^\star, r^\star) \in \omega_m$,*

$$p_m^\star(x^\star, r^\star) = \frac{1}{\ln(R_2/R_1)}\Big((p_d^\star(x^\star) - p_b^\star(x^\star))\ln(Rr^\star) + p_b^\star(x^\star)\ln R_2 - p_d^\star(x^\star)\ln R_1\Big).$$

Moreover, the derivative of $p_m^\star$ with respect to $r^\star$ (which appears in the other equations) reads

$$\partial_{r^\star} p_m^\star(x^\star, r^\star) = \frac{p_d^\star(x^\star) - p_b^\star(x^\star)}{r^\star \ln(R_2/R_1)}.$$

In particular, we can express the fluid velocity in the membrane:

$$u_x^\star(x^\star, r^\star) = 0 \quad \textit{and} \quad u_r^\star(x^\star, r^\star) = -\frac{\widetilde{\mathcal{D}a}}{\mathcal{P}_1}\frac{p_d^\star(x^\star) - p_b^\star(x^\star)}{r^\star \ln(R_2/R_1)}.$$

Remark 3.2 *In the case where the blood is considered as a Newtonian fluid an analytical expression of the simplified system* (8a)-(14d) *can be obtained (see [10] for details).*

Remark 3.3 *By ignoring the terms of order ε, the simplified system does not depend any more of the time. In other words, among other simplifications, we are searching for a stationary solution of the system considered in Appendix A.*

3.4 Different rheological models for blood

As indicated above, the blood is generally considered as a Newtonian fluid, or as well as a quasi-Newtonian fluid. Its viscosity is assumed to be variable and is described by a function G, or, equivalently, by its corresponding dimensionless version $\widetilde{G}$. More precisely, we recall that we have the following relation between the viscosity and the function G:

$$\text{viscosity} = \mu\, G(\dot\gamma),$$

where μ is the reference viscosity and where $\dot{\gamma}$ corresponds to the shear rate. In particular, when the blood is modeled as a Newtonian fluid its viscosity is constant and is given by

$$\mu_\infty = 3.45 \times 10^{-3}\text{Pa.s.} \tag{15}$$

Recalling from Table 2 that the reference viscosity is $\mu = 10^{-3}$Pa.s, it follows that $\widetilde{G}(X) = 3.45$ for this Newtonian model.

In Table 4, different widely used non-Newtonian constitutive relationships for the blood viscosity model against the shear rate are summarized. For more details concerning these non-Newtonian blood viscosity models we refer to [24].

Model	Description
Power-law model	$\widetilde{G}(X) = m\left(\dfrac{\varepsilon^2 P}{\mu}\right)^{n-1} X^{n-1}$
	$m = 4.25$
	$n = 0.7755$
Carreau model	$\widetilde{G}(X) = \dfrac{1}{\mu}\left(\mu_\infty + \left(\mu_0 - \mu_\infty\right)\left(1 + (\lambda^\star X)^2\right)^{\frac{n-1}{2}}\right)$
	$\mu_0 = 0.056\,\text{Pa.s}$
	$\lambda^\star = \dfrac{\varepsilon^2 P}{\mu}\lambda$, with $\lambda = 3.131\,\text{s}$
	$n = 0.3568$
Quemada model	$G(X) = \dfrac{\mu_p}{\mu}\left(1 - \dfrac{1}{2}\dfrac{k_0 + k_\infty\sqrt{X/\gamma^\star}}{1+\sqrt{X/\gamma^\star}}\phi\right)^{-2}$
	$\mu_p = 1.2 \times 10^{-3}\,\text{Pa.s}$
	$\phi = 0.4$
	$k_0 = 4.65$, $k_\infty = 1.84$
	$\gamma^\star = \gamma_c\dfrac{\mu}{\varepsilon^2 P}$, with $\gamma_c = 2.23\,\text{s}^{-1}$
Cross model	$\widetilde{G}(X) = \dfrac{1}{\mu}\left(\mu_\infty + (\mu_0 - \mu_\infty)\left(1 + \left(\dfrac{X}{\gamma^\star}\right)^n\right)^{-1}\right)$
	$\mu_0 = 0.0364$
	$\gamma^\star = \gamma_c\dfrac{\mu}{\varepsilon^2 P}$, with $\gamma_c = 2.63\,\text{s}^{-1}$
	$n = 1.45$

Table 4: Some non-Newtonian blood viscosity models.

In order to compare these rheological models, we numerical computed the minimal and the maximal values of the shear rate $\dot{\gamma}$ appearing along the iterations in the fixed point algorithm used to tackle the non-linearity given by $\widetilde{G}$ (for models listed in this section). We obtained that the values $\dot{\gamma}$ are mainly distributed in the interval $[10^{-4}, 10^2]$. As illustrated in Figure 4, all the considered models, at the exception of Power-low model, are similar to the Newtonian one for values of X close to 10^2, having slightly different behaviors when X goes to zero.

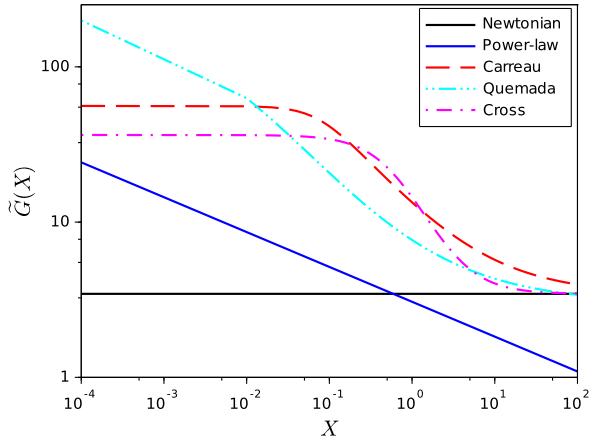

Figure 4: Dimensionless viscosity functions $\widetilde{G}$ for different models (the quantity X corresponding to the dimensionless shear stress).

3.5 Numerical simulations of the flows within a fiber

To numerically approach a solution to the previous systems, we first introduce their weak formulations. For the interested reader, this is postponed in the Appendix B. In order to solve this weak formulation we use the finite element method combined to a fixed point strategy employed for taking into account the non-linearity given by $\widetilde{G}$. We use $\mathbb{P}_1$-bubble finite elements to represent the velocities ($w_x^\star$, $w_r^\star$, $v_x^\star$ and $v_r^\star$) and $\mathbb{P}_1$ finite elements for the pressures ($p_b^\star$ and $p_d^\star$). For the numerical implementation `FreeFem++` [15] is employed.

3.5.1 Effective computations of the flows - the case of pressure data

In the simplest case we assume that all data on Tables 2 and 3 are known, as well as the non-linearity $\widetilde{G}$. For the results in this subsection the geometry of the dialyzer is the one described by the Set A in Table 2. We then compute the non-dimensional numbers, $\mathcal{D}a$, B_b, $\mathcal{P}_1$ and $\mathcal{P}_2$ in order to numerically approach the solution of the variational formulations introduced in Appendix B.

The velocity in the entire domain ω is denoted $(U_x^\star, U_r^\star)$ and is linked to the velocities in the blood, in the membrane and in the dialysate as follows

$$(U_x^\star, U_r^\star) = \begin{cases} (v_x^\star, v_r^\star) & \text{in } \omega_b, \\ (u_x^\star, u_r^\star) & \text{in } \omega_m, \\ (w_x^\star, w_r^\star) & \text{in } \omega_d. \end{cases}$$

We denote (U_x, U_r) the physical velocity and, hence, defined on the real entire physical domain Ω.

Using the boundary values for pressures p_b and p_d prescribed in Table 3, the effects of rheological models proposed in Section 3.4 on the velocity of fluids appearing in our model are illustrated in Figure 5. We remark that the choice of the rheology governing the blood flow has an influence on the horizontal velocity profile in the domain Ω_b and almost no influence on the radial blood flow and on both flows in domains Ω_m and Ω_d.

As a title of example, we choose to illustrate only the Newtonian model and the Power-law model for the rheology of the blood. The pressure and the velocity in the three domains Ω_b, Ω_m and Ω_d, obtained again for the boundary values of pressure p_b and p_d listed in Table 3, are displayed in Figure 6 and Figure 7 respectively. We remark that the pressure profiles are very similar for both models and the velocity in Ω_b shows a more important dependence to the rheology model of the blood.

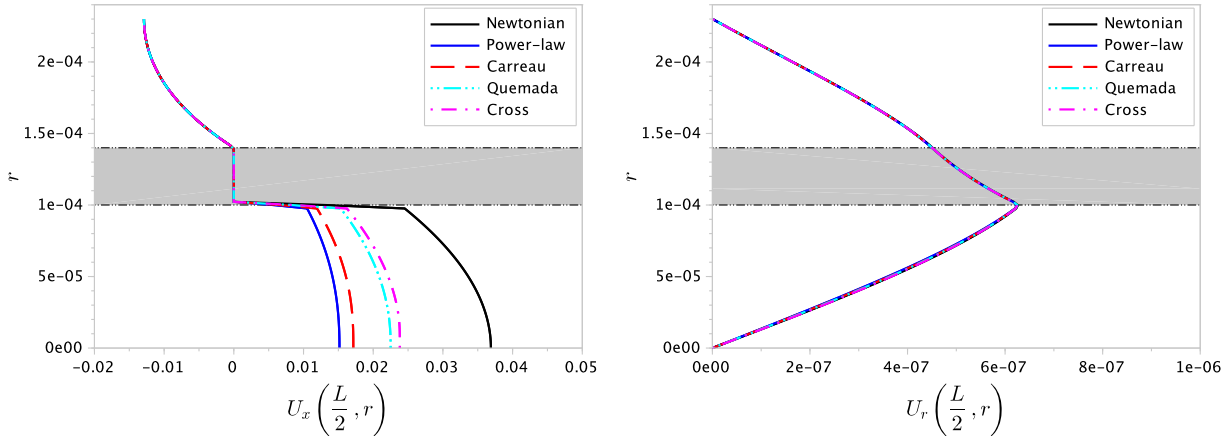

(a) (b)

Figure 5: Velocity profiles on the line $x = \dfrac{L}{2}$ corresponding to geometry parameters in Table 2 (Set A) and pressure boundary data in Table 3. (a) Values (in m.s^{-1}) of the horizontal component of the velocity $U_x(\frac{L}{2}, r)$ for $r \in (0, R)$. (b) Values (in m.s^{-1}) of the radial component of the velocity $U_r(\frac{L}{2}, r)$ for $r \in (0, R)$.

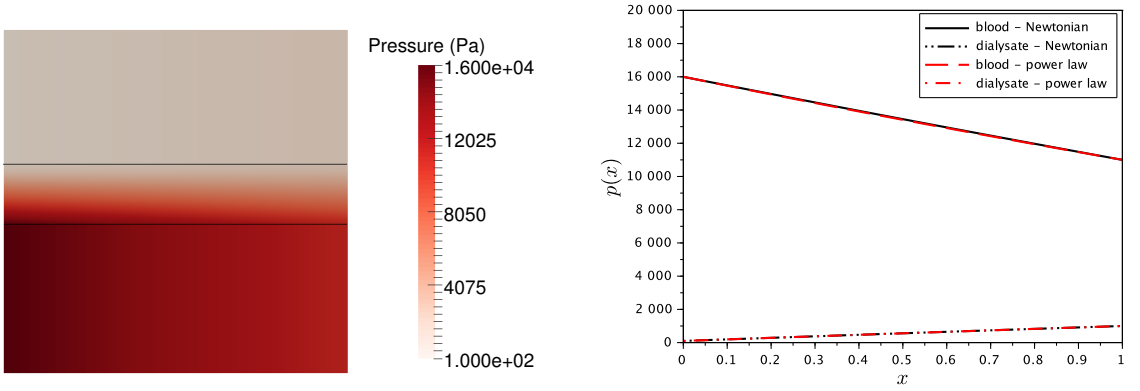

(a) (b)

Figure 6: Pressure (in Pa) corresponding to Power-law model, geometric parameters in Table 2 and boundary values in Table 3. (a) Spatial distribution in domain Ω. (b) Longitudinal profile of pressure in blood and dialysate.

We mention that we obtained very similar flow rates for the blood and dialysate as the ones previously obtained in [8] for the same choice of pressure data, the same geometry and a similar blood rheology.

3.5.2 Effective computations of the flows - the case of flow rates data

In a more complex case from a numerical point of view, but a more natural one from an experimental point of view, the pressures at the entrance and at the exit of domains Ω_b and Ω_d ($\vec{P} = (p_{b,\text{in}}, p_{b,\text{out}}, p_{d,\text{in}}, p_{d,\text{out}})$) are not available, but we only dispose of the fluxes $\vec{Q}$ at the entrance and at the exit of dialyser. Since the number of fibers composing the dialyser and their geometry are known, we can easily deduce from

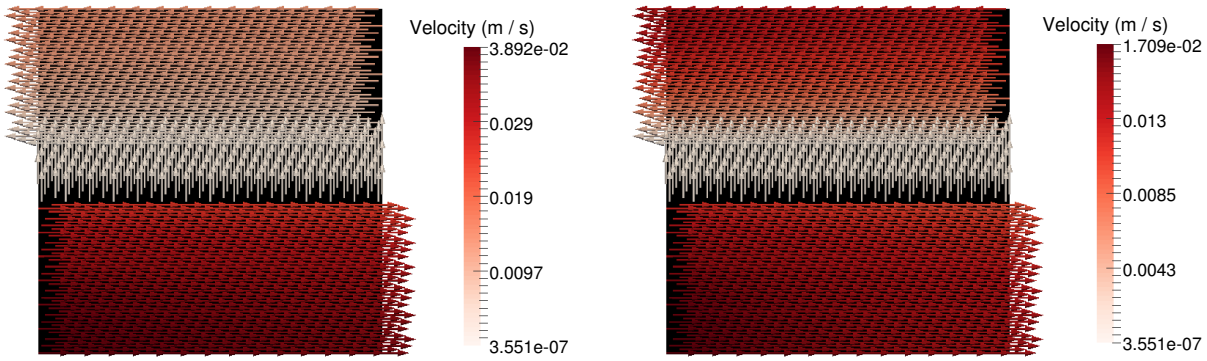

(a) (b)

Figure 7: Velocity magnitude of fluids in Ω corresponding to Newtonian model (a) and Power-law model (b), geometric parameters in Table 2 Set A and pressure boundary data listed in Table 3.

the fluxes $\vec{Q} = (Q_{b,\text{in}}, Q_{b,\text{out}}, Q_{d,\text{in}}, Q_{d,\text{out}})$ the fluxes at the entrance and exit of domains Ω_b and Ω_d. An example of such fluxes is given in Table 5. These flow rates are directly defined from the velocity field.

Name	Notation	EX1 (ml.min^{-1})	EX2 (ml.min^{-1})
Blood injection flux	$Q_{b,\text{in}}$	300	400
Blood output flux	$Q_{b,\text{out}}$	290	390
Dialysate injection flux	$Q_{d,\text{in}}$	500	500
Dialysate output flux	$Q_{d,\text{out}}$	510	510

Table 5: Typical values for the fluxes for clinical dialysis

For instance, the blood flux at the entrance of the domain Ω_b is related to the blood injection flux by the following relation:

$$Q_{b,\text{in}} = 2\pi N \int_0^{R_1} v_x(0,r) r \, \mathrm{d}r,$$

where N is the number of hollow fibers composing the dialyser. It is therefore relatively easy to determine the fluxes $\vec{Q}$ from the pressures $\vec{P}$ using the procedure proposed above; we denote Φ the application associating to a given pressure vector $\vec{P}$ the corresponding fluxes vector $\vec{Q}$. The reverse is much less obvious. We propose an optimization algorithm to determine the pressures from the fluxes. Given the flow rates $\vec{Q}$ we will minimize the following function:

$$\mathcal{J}(\vec{P}) = \frac{1}{2}\|\Phi(\vec{P}) - \vec{Q}\|^2, \tag{16}$$

where $\|\cdot\|$ is the usual euclidean norm on $\mathbb{R}^4$. In this purpose, we implemented a gradient-type algorithm described in Appendix C (in practice, this algorithm is used with the following numerical parameters: $h = \varepsilon_1 = 1$, and $\alpha_0 = 10^3$).

With the flux data instead of the pressure data (that is using Table 5 instead of Table 3), we compute the velocity of the fluids for the rheological models proposed in Section 3.4. The vertical and horizontal velocity profiles obtained for different blood rheologies and for pressures data (EX1) are illustrated in Figure 8. The results in this subsection correspond to a dialyzer described by the Set B in Table 2.

Remark 3.4 *Contrarily to the results illustrated in Figure 5 (a), we observe that the longitudinal velocities displayed in Figure 8 (a) present much less variation with respect to the choice of the model. This is a consequence of the fact that for the simulations in Figure 8, for each one of the rheologies considered in this paper, the values of the blood and dialysate input and output pressures were chosen such that the blood and dialysate flow rates match the values listed in Table 5. Therefore, the influence of the rheology is much less visible than in the case considered for Figure 5 where the pressure data was the same for each rheology.*

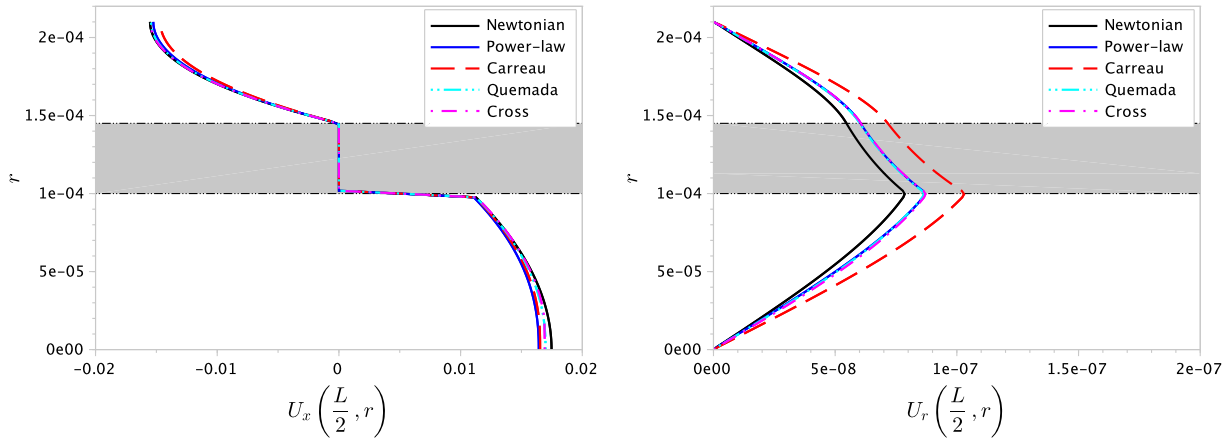

(a) (b)

Figure 8: Velocity profiles on the line $x = \dfrac{L}{2}$ corresponding to geometry parameters in Table 2 (Set B) and pressures boundary data optimized to match the flows in Table 5 (EX1). (a) Values (in m.s^{-1}) of the horizontal component of the velocity $U_x(\frac{L}{2}, r)$ for $r \in (0, R)$. (b) Values (in m.s^{-1}) of the radial component of the velocity $U_r(\frac{L}{2}, r)$ for $r \in (0, R)$.

The longitudinal profiles of pressure in blood and in dialysate corresponding to a Newtonian model and for boundary pressure data optimized in order to minimize the functional $\mathcal{J}$ given by (16) are displayed in Figure 9. We observe that these profiles are qualitatively different to the ones in Figure 6 (b) which correspond to pressure boundary data in Table 3. More exactly, the pressure $p_{b,out}$ of the blood at the exit of the dialyzer is smaller than the pressure $p_{d,in}$ of the dialysate at the entrance of the dialyzer. This is surprinsing with respect to previous literature (see, for instance, [8, 7, 10]) were is often assumed that $p_{b,out} > p_{d,in}$ and in the same time is in complete agreement with the pressure values observed for a standard hemodialysis session and listed in Table 10.

4 Evolution of chemicals in blood and dialysate during dialysis

In this section we describe a model for the evolution of concentrations of several chemical components of blood and dialysate during a dialysis process. Since we are interested in the study of the calcium balance during hemodialysis using a citrate containing dialysate, we propose to use a transport–diffusion–reaction equation for a number of five chemical species described in subsection 4.3. A similar model was employed for the study of the dynamic exchange of bicarbonate and the exchange of sodium during dialysis, respectively, [1, 2] and [32].

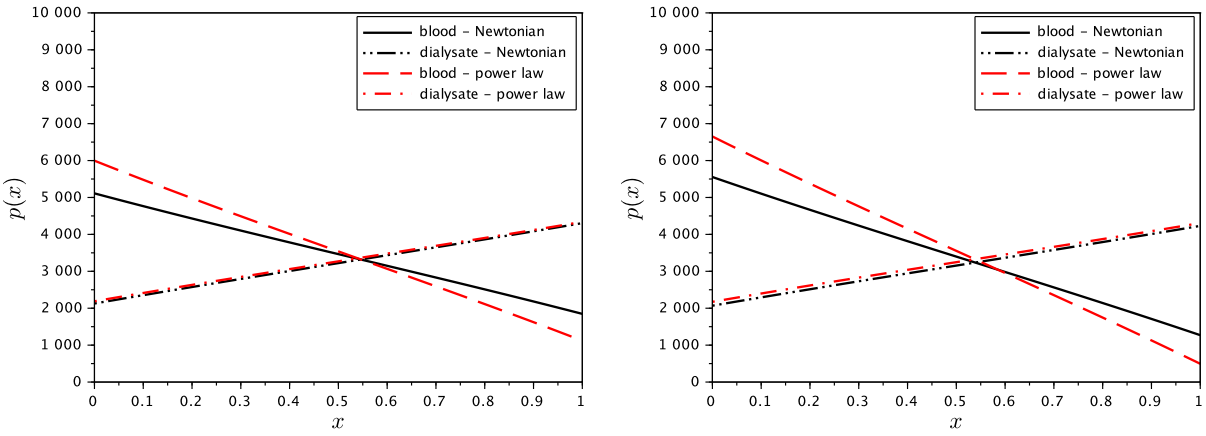

(EX1) (EX2)

Figure 9: Longitudinal profile of pressure in blood and dialysate corresponding to geometry parameters in Table 2 (Set B) and pressures boundary data optimized to match the flows in 5 (EX1) and (EX2).

4.1 Transport diffusion process

The solute concentration mechanism which is coupled to the velocity field (U_x, U_r) is modeled by a convection–diffusion–reaction equation. More precisely, for any species (whose the concentration is denoted c_i, $i = 1, ..., 5$), we have for every $(x, r) \in \Omega$ and $t > 0$

$$\underbrace{\partial_t c_i}_{\text{transient}} + \underbrace{S_i(U_x \partial_x c_i + U_r \partial_r c_i)}_{\text{transport}} - \underbrace{\frac{1}{r}\partial_r(r D_i \partial_r c_i) - \partial_x(D_i \partial_x c_i)}_{\text{diffusion}} = \underbrace{F_i(c_1, ..., c_5)}_{\text{reaction}}. \tag{17}$$

The quantities D_i represent the diffusion coefficients ($\mathrm{m}^2.\mathrm{s}^{-1}$) and they depend on the species i. The coefficients S_i are the so called sieving coefficients. A sieving coefficient equal to 1 corresponds to unhindered solute transport: it is naturally the case in blood or in dialysate domains. In the membrane, in order to take into account the size of the molecules, we impose that the sieving coefficients are equal to zero for large proteins like Albumin (see [7]). The reaction source terms F_i model the interaction between different species. They will be precised later (see subsection 4.3).

4.2 Boundary conditions for the concentrations

In order to complete the system (17) we should impose some boundary conditions on the concentrations $(c_i)_{1 \le i \le 5}$. Therefore, we assume known each concentration c_i in the blood and in the dialysate fluid at the entrance of the dialyzer. Indeed, since the dialysate composition is provided by its producer and the concentrations in the blood can be obtained by *a priori* measurements, this assumption is reasonable and translates into the following Dirichlet boundary conditions:

$$c_i = c_{i,\ell} \quad \text{on} \quad \Gamma_{\ell,b} \qquad \text{and} \qquad c_i = c_{i,r} \quad \text{on} \quad \Gamma_{r,d}. \tag{18}$$

On the remaining part of the boundary of Ω the concentrations are unknown. A natural assumption is that the concentrations are constant in a neighborhood of the boundary and in a direction perpendicular to the boundary. This hypothesis translates into the following Neumann boundary conditions:

$$\begin{cases} \partial_x c_i = 0 \quad \text{on} \quad \Gamma_{\ell,d} \cup \Gamma_{\ell,m} \cup \Gamma_{r,m} \cup \Gamma_{r,b}, \\ \partial_r c_i = 0 \quad \text{on} \quad \Gamma_b \cup \Gamma_d. \end{cases} \tag{19}$$

Remark 4.1 *For system* (17) *domain* Ω *is considered without the two interior boundaries* Γ_{bm} *and* Γ_{md} *separating the flow domains. That is possible because all the quantities appearing in* (17) *are defined over the entire domain* Ω*. Indeed, the velocity field* (U_x, U_r) *even it has been modelled using different equations for different flow domains, in the end is defined everywhere. The diffusion coefficients* D_i *and the sieving coefficients* S_i *have different values for the blood, for the membrane and for the dialysate, but, even if these coefficients are discontinuous, the variational formulation associated to* (17) *is well posed on the whole domain* Ω*.*

4.3 Biochemical reactions

In this paper, we are interested on the complex formed by the Calcium, the Albumin and the Citrate. The equilibrium reactions for these species can produce the Calcium–Albumin as follows:

$$\text{Calcium} + \text{Albumin} \underset{k_2}{\overset{k_1}{\rightleftharpoons}} \text{Calcium–Albumin},$$

where the reaction rate constants are denoted k_1 and k_2. We also note that Albumin has 12 binding sites for Calcium. The equilibrium reactions can also produce the Calcium–Citrate as follows:

$$\text{Calcium} + \text{Citrate} \underset{k_4}{\overset{k_3}{\rightleftharpoons}} \text{Calcium–Citrate},$$

where the reaction rate constants are denoted k_3 and k_4. Equilibrium constants were retrieved from literature data [27, 29, 22, 14]. Reaction rate constants k_i are more difficult to measure and fewer data are available. In this case we assume that the studied chemical reactions follow a first order kinetics. The first rate constant is fixed arbitrarily (its magnitude is chosen according to the data available with similar reactions), the other constants being calculated such that their ratio is equal to the equilibrium constant. The values of the reaction constants used in this paper are given by:

$$\begin{aligned} k_1 &= 1\,\text{mol.m}^3\text{.s}^{-1}, & k_2 &= 10\,\text{s}^{-1}, \\ k_3 &= 0.28\,\text{mol.m}^3\text{.s}^{-1}, & k_4 &= 0.15\,\text{s}^{-1}. \end{aligned}$$

Consequently, we consider five species those concentrations c_i are listed in Table 6.

c_1	concentration of free Calcium
c_2	concentration of free Albumin binding sites for Calcium
c_3	concentration of occupied Albumin binding sites for Calcium
c_4	concentration of Citrate
c_5	concentration of Calcium–Citrate

Table 6: Chemical species considered in the convection–diffusion–reaction process.

Since molecules of Albumin do not traverse the membrane, their corresponding sieving coefficients are given by

$$S_i(x) = \begin{cases} 1 & \text{if } x \in \Omega_b \cup \Omega_d \\ 0 & \text{if } x \in \Omega_m, \end{cases} \qquad \text{for } i \in \{2, 3\}$$

and all other sieving coefficients S_1, S_4 and S_5 are identically equal to one in Ω. Diffusion coefficients in blood and dialysate domains were assumed to be equal to diffusion coefficient in free water. Diffusion

coefficients in free water were retrieved from literature data [28, 30, 34]. When diffusion coefficients in water at the temperature 310K were not available they were calculated according to the Einstein relation. Diffusion coefficients in membrane were assumed to be five times smaller than in water as they can be measured for other solutes (see, for instance [8]). The values of the diffusion coefficients D_i at the temperature 310K are gathered in Table 7.

Name	Notation	Value ($m^2.s^{-1}$)
Reference diffusion	D	10^{-10}
Calcium diffusion	D_1	16.6×10^{-10}
Albumin diffusion	D_2 and D_3	0.877×10^{-10}
Citrate and Calcium-Citrate diffusion	D_4 and D_5	7.6×10^{-10}

Table 7: Typical values for the diffusion coefficients.

Typical values for the concentrations in which we are interested for are calculated according to the mass action law from data in the literature [27, 5, 3] and are listed in the Table 8. We consider three dialysates having different concentrations of calcium and citrate. The concentrations provided by the manufacturer (Citrasate ®) are listed in Table 9. These values appear as boundary conditions in (19).)

Name	Notation	Value ($mol.m^{-3}$)
Reference concentration	C	1
Free Calcium	$c_{1,\ell}$	1.2
Free Albumin sites	$c_{2,\ell}$	6.53
Calcium–Albumin sites	$c_{3,\ell}$	0.783
Citrate	$c_{4,\ell}$	3.07×10^{-2}
Calcium–Citrate	$c_{5,\ell}$	6.93×10^{-2}

Table 8: Typical values for the concentration data in blood at the inlet of the hallow fiber (on $\Gamma_{\ell,b}$).

Name	Notation	Dialysate $\mathcal{D}_0$	Dialysate $\mathcal{D}_1$	Dialysate $\mathcal{D}_2$
Calcium	$c_{1,r}$	1.5	9.81×10^{-1}	1.11
Free Albumin sites	$c_{2,r}$	0	0	0
Calcium–Albumin sites	$c_{3,r}$	0	0	0
Citrate concentration	$c_{4,r}$	0	2.81×10^{-1}	2.6×10^{-1}
Calcium–Citrate	$c_{5,r}$	0	5.19×10^{-1}	5.4×10^{-1}

Table 9: Concentrations (in $mol.m^{-3}$) for three dialysate fluids (on $\Gamma_{r,d}$).

Within this notation, the reaction source terms F_i are then described by the following relations:

$$F(c_1,...,c_5) = \begin{pmatrix} k_2c_3 + k_4c_5 & - & k_1c_1c_2 - k_3c_1c_4 \\ k_2c_3 & - & k_1c_1c_2 \\ -k_2c_3 & + & k_1c_1c_2 \\ k_4c_5 & - & k_3c_1c_4 \\ -k_4c_5 & + & k_3c_1c_4 \end{pmatrix}.$$

4.4 Scaling procedure

Since the reference velocity in the blood (V) and the reference velocity in the membrane/dialysate (W) are different, we must choose a common reference velocity for the dialyser. In practice, the complete velocity field (U_x, U_r) is written using the characteristic velocity V. More precisely, we introduce the non-dimensional velocity $(U_x^\star, U_r^\star)$ such that

$$U_x = V\,U_x^\star \quad \text{and} \quad U_r = \varepsilon V\,U_r^\star.$$

Moreover, we need to introduce characteristic sizes for the concentrations c_i, for the diffusion coefficients D_i and for the source terms F_i (we choose k_2 as reference rate constant):

$$c_i = C\,c_i^\star, \quad D_i = D\,D_i^\star, \quad F_i = k_2\,C\,F_i^\star.$$

In the rescaled domain, and, therefore, for every $(x^\star, r^\star) \in \omega$ and $t^\star > 0$, the equation becomes:

$$\partial_{t^\star} c_i^\star + S_i\,(U_x^\star \partial_{x^\star} c_i^\star + U_r^\star \partial_{r^\star} c_i^\star) - \frac{1}{\mathcal{P}e}\frac{1}{r^\star}\partial_{r^\star}(r^\star D_i \partial_{r^\star} c_i^\star) - \frac{\varepsilon^2}{\mathcal{P}e}\partial_{x^\star}(D_i \partial_{x^\star} c_i^\star) = \frac{1}{\mathcal{F}d} F_i^\star(c_1^\star,...,c_5^\star), \qquad (20)$$

and the reaction source term is given by

$$F^\star(c_1^\star,...,c_5^\star) = \begin{pmatrix} c_3^\star + \delta_2 c_5^\star & - & \delta_1 c_1^\star c_2^\star - \delta_3 c_1^\star c_4^\star \\ c_3^\star & - & \delta_1 c_1^\star c_2^\star \\ -c_3^\star & + & \delta_1 c_1^\star c_2^\star \\ \delta_2 c_5^\star & - & \delta_3 c_1^\star c_4^\star \\ -\delta_2 c_5^\star & + & \delta_3 c_1^\star c_4^\star \end{pmatrix}.$$

Note that we have introduced five supplementary non-dimensional numbers:

$$\mathcal{P}e = \frac{R^2\,V}{L\,D}, \qquad \mathcal{F}d = \frac{V}{L\,k_2}, \qquad \delta_1 = \frac{k_1\,C}{k_2}, \qquad \delta_2 = \frac{k_4}{k_2} \quad \text{and} \quad \delta_3 = \frac{k_3\,C}{k_2}.$$

Using the parameters given in Table 2 Set B, Table 7, Table 8 and input pressures optimized in order to match the flow rates in Table 5 EX1, the following values are obtained for the model parameters:

$$\mathcal{P}e \approx 588, \qquad \mathcal{F}d \approx 0.133, \qquad \delta_1 = 10^{-1}, \qquad \delta_2 = 1.5 \times 10^{-2} \quad \text{and} \quad \delta_3 = 2.8 \times 10^{-2}.$$

Even if the Péclet's number $\mathcal{P}e$ is of order of $1/\varepsilon$ we prefer to keep the term $\frac{1}{\mathcal{P}e}\frac{1}{r^\star}\partial_{r^\star}(r^\star D_i \partial_{r^\star} c_i^\star)$ in (20). In fact, this term has a regularizing effect for the solutions $(c_i)_{1\le i\le 5}$ and that is important particularly for discontinuous initial concentrations.

Finally, the boundary conditions become

$$\begin{cases} \partial_{x^\star} c_i^\star = 0 & \text{on} \quad \gamma_{\ell,d} \cup \gamma_{\ell,m} \cup \gamma_{r,m} \cup \gamma_{r,b}, \\ \partial_{r^\star} c_i^\star = 0 & \text{on} \quad \gamma_b \cup \gamma_d, \\ c_i^\star = c_{i,\ell}/C & \text{on} \quad \gamma_{\ell,b}, \\ c_i^\star = c_{i,r}/C & \text{on} \quad \gamma_{r,d}. \end{cases}$$

We complete this system by the following initial condition:

$$c_i^\star(x^\star, 0) = c_i^{0,\star}(x^\star) = \begin{cases} c_{i,\ell}/C & \text{if } x^\star \in \omega_b, \\ c_{i,r}/C & \text{if } x^\star \in \omega_m \cup \omega_d, \end{cases}$$

for $i \in \{1,\ 2,\ 3,\ 4,\ 5\}$.

4.5 Variational formulation and numerical approach

In a first step, we consider the variational formulation of (20) detailed at the end of Appendix B.

We use an implicit one step discretization scheme in time and the finite elements method for the space discretization. Moreover, in order to obtain a faster numerical solver, we compute one concentration $c_i^\star$ at a time, replacing the unavailable concentrations at the current time step by their values at the previous time step. For a given time $t^\star > 0$ concentrations $c_i^\star(t^\star, x^\star, r^\star)$ are represented using $\mathbb{P}_1$ finite elements and `FreeFem++` is used for the numerical implementation.

For every time $t^\star > 0$, we denote $E(t^\star)$ the following quantity associated to the evolution in time of concentrations $c_i^\star(t^\star, \cdot, \cdot)$ and defined by

$$E(t^\star) = \left(\sum_{i=1}^{5} \iint_\omega r^\star \left| c_i^\star(t^\star, x^\star, r^\star) \right|^2 \mathrm{d}x^\star \mathrm{d}r^\star \right)^{\frac{1}{2}} \quad \text{for every } t^\star > 0. \tag{21}$$

Let $E'(t^\star)$ be the derivative with respect to the time $t^\star$ of the function E. It is easy to remark that when concentrations $(c_i^\star(t^\star))_{1 \le i \le 5}$ approach to a stationary solution $E'(t^\star)$ is close to zero. For all the simulations in Section 5 we choose a time interval $(0, T^\star)$, on which we compute the concentrations $c_i^\star$, such that $E'(T^\star) \le 10^{-4}$.

5 Numerical experiments

Pressure measurements were effectuated on an APS18 dialyser for a dialysate input flux of $500\,\mathrm{ml.min^{-1}}$ and an ultra-filtration flux equal to $10\,\mathrm{ml.min^{-1}}$. Pressure values were recorded, using pressure sensors situated at the level of the input and exit of blood and dialysate tubes respectively. The values for two different input blood fluxes are listed in Table 10. The pressures at the level of hollow fiber (our computation domain) were numerically computed by the optimization method proposed in the subsection 3.5.2 such that the corresponding flows are the one indicated in Table 5.

The APS18 dialyzer has a diameter of 4.2 cm and it is composed of a number of $N = 10^4$ fibers with a inner channel having a radius of 10^{-4} m and a wall thickness of hollow fibers of 0.45×10^{-4} m. The length of such a dialyser is 33 cm. Remark that these values are exactly the same as those listed in Table 2 Set B.

5.1 Concentrations for blood modelled as a Newtonian fluid

The spatial concentrations for all considered species at a (no-dimensional) time $T^\star$ such that $E'(T^\star) < 10^{-4}$ obtained for the flows given by (EX1) are displayed in Figure 10. More precisely, for all the numerical

	Input blood flux	Blood input pressure	Blood output pressure	Dialysate input pressure	Dialysate output pressure
(EX1)	300 ml.min^{-1}	200	110	200	95
(EX2)	400 ml.min^{-1}	276	164	262	58

Table 10: Values of input and output pressures (in mmHg) for a dialysate flux of 500 ml.min^{-1} and an ultrafiltration flux of 10 ml.min^{-1}.

experiments we choose $T^\star = 300T$ which corresponds to a real time of 300s and verifies the condition $E'(T^\star) < 10^{-4}$. This value of $T^\star$ is a good compromise between the computational cost and the reach of the equilibrium in the chemical reactions.

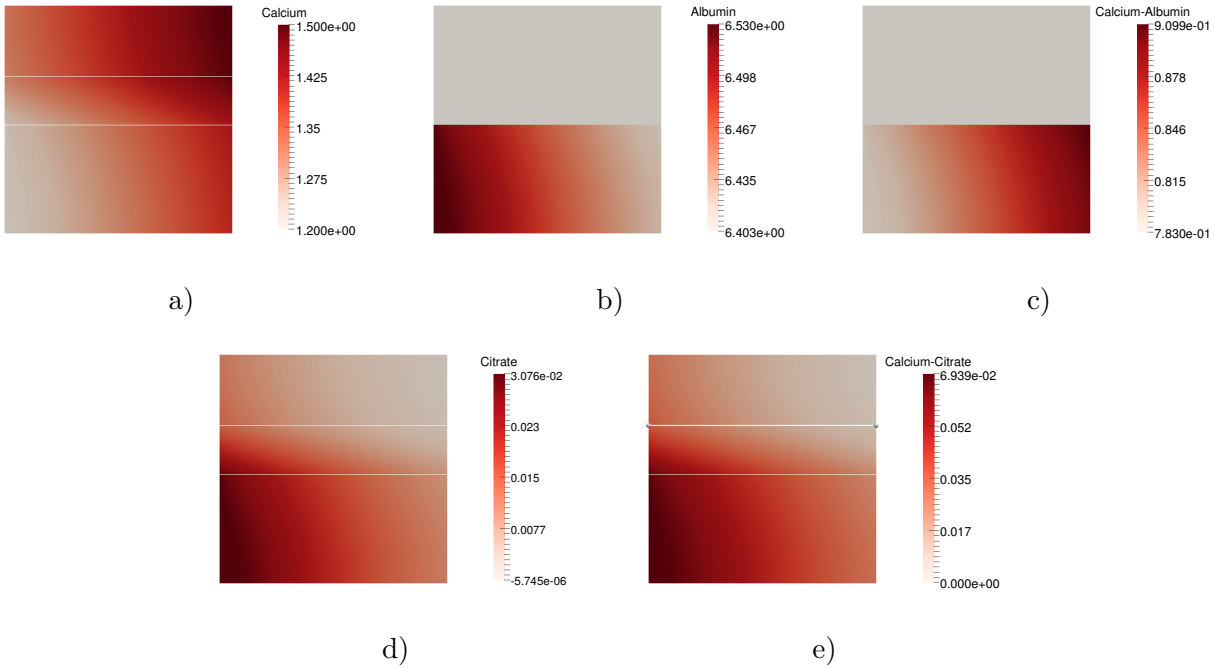

Figure 10: Concentrations c_i (in mol.m^{-3} or, equivalently, in mmol.l^{-1}) in domain ω at a non-dimensional time T^* corresponding to approximately 300s of real time and for (EX1) and dialysate $\mathcal{D}_0$. a) Calcium. b) Free Albumin binding sites for Calcium. c) Calcium-Albumin sites. d) Citrate. e) Calcium-Citrate.

In Figure 10 we remark that the concentrations computed by the model are smooth enough and that the imposed boundary conditions are well satisfied. We also remark an increase of the Calcium concentrations in the blood at the exit of the dialyzer.

In order to analyze the evolution of concentration for different molecules considered here we define the mean concentrations in the output blood $\overline{c}_i(t)$ at the time t by

$$\overline{c}_i(t) = \frac{2R^2}{R_1^2} \int_0^{\frac{R_1}{R}} r\, c_i(t, 1, r)\, \mathrm{d}r.$$

In Figure 11 we can follow the evolution in time of the concentration $\overline{c}_1(t)$ of free Calcium in the blood at the dialyser's outlet for a velocity field computed in order to fulfill the flow rates in Table 5 (EX1) and

two different blood rheologies: for the first the blood is modelled as a Newtonian fluid and the second one consider the blood a non-Newtonian fluid. More exactly, we used the Power-low model. The blood composition at the dialyzer's inlet is described in Table 7 and the three dialysates $\mathcal{D}_0$, $\mathcal{D}_1$ and $\mathcal{D}_2$ are described in Table 8. Remark that, since at $T^\star = 300T$ the value $E'(T^\star)$ is relatively small, the mean concentrations of free Calcium in the blood at the exit of dialyser reached their stationary values. A similar comportment was observed for all other chemical species considered by the model.

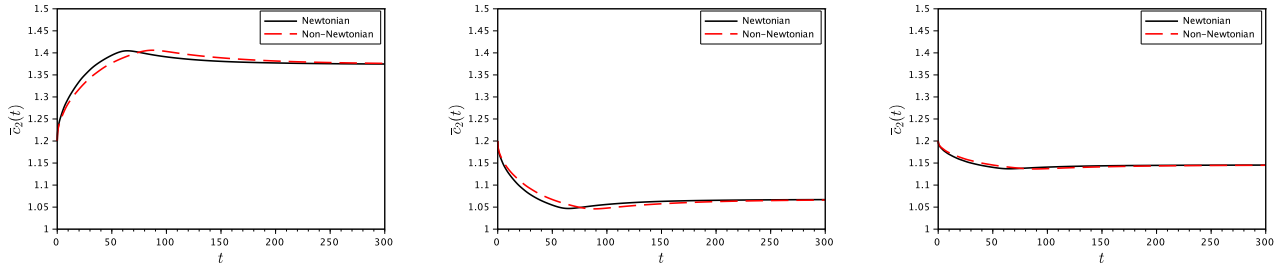

(a) (b) (c)

Figure 11: Evolution of the concentration $\overline{c}_1(t)$ (in mol.m^{-3} or, equivalently, in mmol.l^{-1}) of free Calcium in blood at the exit of dialyser for dialysate fluids described in Table 9. (a) Dialysate $\mathcal{D}_0$. (b) Dialysate $\mathcal{D}_1$. (c) Dialysate $\mathcal{D}_2$.

The spatial distribution of the Calcium concentration corresponding to the final time associated to the simulations illustrated in Figure 11 are displayed in Figure 12. More precisely, in this figure we display the spatial distribution of the Calcium concentration c_1 associated to flow-rates (EX1) and boundary concentrations in Tables 7 and 8 at the time T^* corresponding to a real time equal to 300s. In order to compare the results obtained for both flows (EX1) and (EX2), the longitudinal profiles of the Calcium concentration at the end of the simulation for all three dialysates in Table 8 are represented in Figure 13.

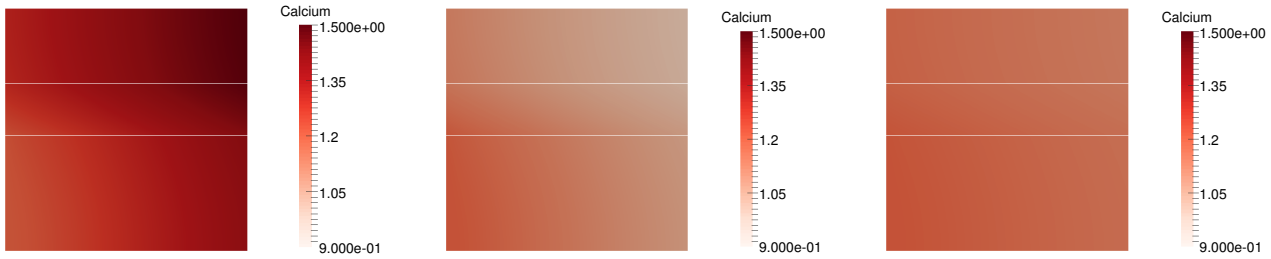

(a) (b) (c)

Figure 12: Spatial distribution of the concentration c_1 (in mol.m^{-3} or, equivalently, in mmol.l^{-1}) of free Calcium at the time 300 s for dialysate fluids described in Table 9. (a) Dialysate $\mathcal{D}_0$. (b) Dialysate $\mathcal{D}_1$. (c) Dialysate $\mathcal{D}_2$.

A quantity of clinical interest is the concentration of total Calcium in the blood at the dialyzer's outlet. In Figure 14 we display the evolution of the concentration of total Calcium $\overline{c}(t) = \overline{c}_1(t) + \overline{c}_3(t) + \overline{c}_5(t)$ in the blood at the exit of the dialyzer. We observe that when using a citrate dialysate, the transfer of calcium from the dialysate to the blood is decreased. For the same calcium concentration in the blood at the inlet of the dialyzer, the total calcium concentration in the blood at the outlet is lesser when the dialysate contains citrate.

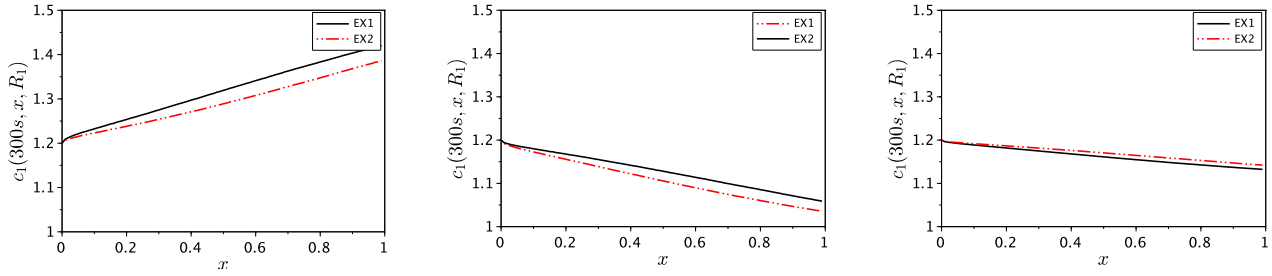

(a) (b) (c)

Figure 13: Longitudinal distribution of the concentration $\overline{c}_1(t)$ (in mol.m^{-3} or, equivalently, in mmol.l^{-1}) of free Calcium in blood at the blood/membrane interface at time $300s$ for dialysate fluids described in Table 9. (a) Dialysate $\mathcal{D}_0$. (b) Dialysate $\mathcal{D}_1$. (c) Dialysate $\mathcal{D}_2$.

(EX1) (EX2)

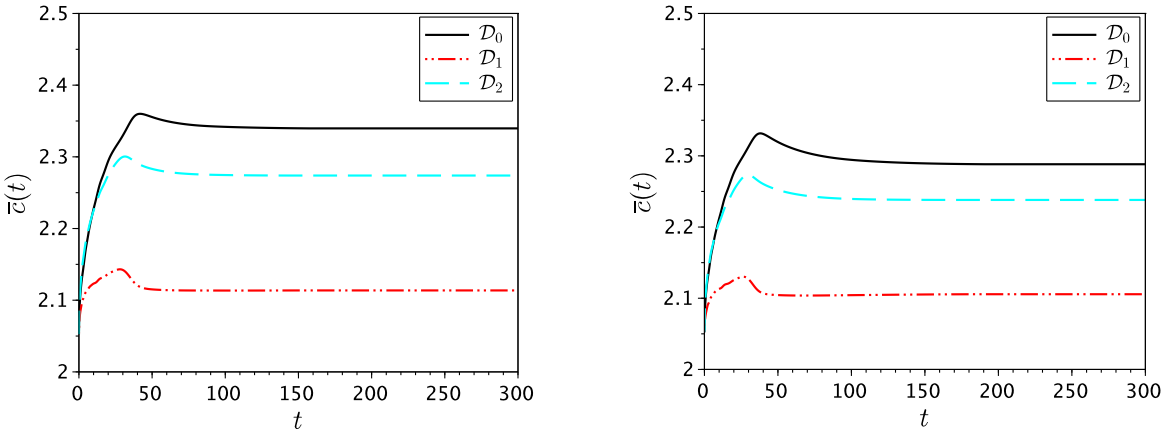

Figure 14: Evolution of the concentration of total Calcium in blood at the exit of the dialyzer for flow data in Table 9 and dialysates $\mathcal{D}_0$, $\mathcal{D}_1$ and $\mathcal{D}_2$.

5.2 Concentrations for blood modelled as a Non-Newtonian fluid

In this section the velocity field (U_x, U_r) is computed using a non-Newtonian model for the blood. Since we are interested on the influence of the blood's rheology on the evolution of the concentrations for chemical species listed in Table 6, we only considered here the Power-law model which seems to provide the results less similar to the Newtonian case.

As in the Newtonian case we stop the numerical experiments at the time $T^\star = 300\,T$ for which the values $E'(T^\star)$ is acceptably small. We recall that this time corresponds to 300 s.

In order to compare the evolution of concentrations for the Newtonian and Non-Newtonian blood flows, Figure 15 displays the evolution of the concentration of free Calcium in blood at the exit of the dialyser for the first five minutes of the dialysis. Small differences can be observed for small values of the time t, the concentration $\overline{c}_1$ arriving at the same stationary solution for both types of flows. These differences are due to the different values of the reference velocity V for each rheology, and, hence, are due to the dependence of the reference time T to the rheology. Nevertheless, for large values of the time T we remark a very small influence of blood's rheology on the concentrations for different chemical species considered by the model.

(EX1) (EX2)

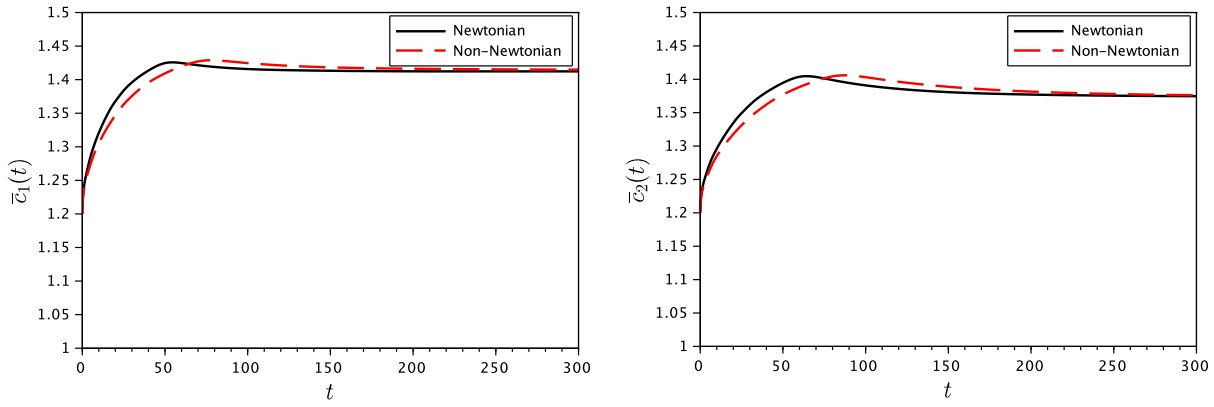

Figure 15: Mean concentration of free Calcium $\bar{c}_1$ (in mol.m^{-3} or, equivalently, in mmol.l^{-1}) in blood at the exit of the dialyser for Newtonian and Non-Newtonian (Power-law) blood flows for (EX1) and (EX2).

6 Conclusion and perspectives

This modeling provides two interesting results for clinical practice. First, the decrease in free calcium concentration in blood is insufficient to explain the anticoagulant effect of citrate containing dialysate. With a citrate-free dialysate, the free calcium concentration of the blood increases between the inlet and the outlet of the dialyzer. Conversely, with a citrate containing dialysate, the free calcium concentration decreases (see Figure 13). However, on contact with the membrane the free calcium concentration remains higher than the concentrations inhibiting coagulation which are below 0.4 mmol.l^{-1} [9]. The modest anticoagulant effect of citrate containing dialysate could be related with its inhibitory effect on complement system and this effect could be increased by using a calcium-free and citrate containing dialysate and injecting a calcium solution into the blood after it leaves the dialyzer. [17].

Secondly, when using a citrate dialysate, the transfer of calcium from the dialysate to the blood is decreased. For the same calcium concentration in the blood at the inlet of the dialyzer, the total calcium concentration in the blood at the outlet is lesser when the dialysate contains citrate (see Figure 14). This is due to a calcium-citrate diffusivity that is smaller than free calcium. The decrease in calcium intake can explain the increased risk of secondary hyperparathyroidism in patients with citrate dialysate [23]. This modeling predicts that a citrate dialysate containing 1.65 mmol.l^{-1} of calcium provides a calcium transfer to the patient equivalent to that obtained with a citrate-free dialysate containing 1.5 mmol.l^{-1} of calcium. In order to maintain the same calcium intake the dialysate calcium concentration must be increased by 0.15 mmol.l^{-1} when using a citrate dialysate. This is an important issue to be considered in clinical practice. Indeed, calcium balance acts directly on bone and mineral disorders in hemodialysis patients.

Concerning the mathematical model, we observed that the choice of blood rheology has a small influence on the evolution of the mean concentrations at the dialyzer outlet or on the concentrations at the level of the membrane. An explanation for that is that we apply an optimization algorithm in order to choose the boundary conditions on the blood and dialysate pressures at the inlet and outlet of a hollow fiber such that the corresponding flow rates match the flow rates measured on the dialyzer. This methodology allow us to consider some very standard boundary conditions for the fluid model. Therefore, once the boundary data on the pressure are computed, the blood can be assumed to be a Newtonian fluid and velocity fields can be computed numerically or even explicitly [10]. The velocity field obtained by solving the fluid model by a finite elements method acts as an input for the convective part in the convection-diffusion-reaction system modelling the evolution of five chemical species presented in blood and in the

dialysate fluid. Since, from a clinical point of view, is interesting to know to concentration of calcium ions at the level of the interface blood/membrane, we considered only the five chemical species in the complex formed by calcium, albumin and citrate. The model can be easily enriched in order to take into account a larger number of chemical species and this will be the subject of a future work.

Our study has several limitations. First, the rate constants of the chemical reactions used to model the interaction between calcium, citrate and albumin do not take into account the changes due to possible variations in the pH of the dialysate and the blood. However, at least for the citrate and calcium reaction, it appears that the change in pH has no influence on the equilibrium constants. Chemical equilibrium is reached much more quickly than other physical phenomena involved. Thus, the exact value of the rate constants has little significance provided that their ratio (equilibrium constant) is right [25]. Also, we have not taken into account the electrical migration phenomenon. The different ion diffusion rates lead to the appearance of an electric field. However this mechanism plays a minor role in the solute flux in the dialyzer notably with the new polysulfone membranes [35]. Finally, this model does not take into account that the oncotic pressure depends on the concentrations of solutes and it is supposed to variate linearly with respect to the longitudinal variable. In order to take into account the dependence of the oncotic pressure to the solute concentration in blood we should consider a model with a stronger coupling between the equation describing the fluid flows and the ones modelling the transport of solutes. This will be the subject of further work.

Knowledge of calcium ions flows and concentrations in the dialyser is necessary for an optimal management of hemodialysis patients. Modelling offers the opportunity to know these data that are not easily measurable. The partial differential equations model and the finite elements method used in our work offer the possibility to describe diffusion and convection but also the chemical reactions between several solutes. Similarly, to calcium ions, it could be adapted to describe and optimize the purification of uremic toxins bound to albumin.

A Dimensionless equations

The goal of this first appendix is to present the non-dimensional form of the equations describing the hydrodynamic flow (see Section 3.1). More precisely, we rewrite all the equations introduced in this section using the changes of variable given page 9. Consequently, all quantities should be marked with an asterisk but for the sake of clarity, in this appendix, we drop asterisks.

For every $t > 0$ and $(x, r) \in \omega_b$, the dimensionless equations governing the blood flow read as follows (see the subsection 3.1.1 for the dimensional form of these equations):

$$\begin{cases} \varepsilon \mathcal{R}e\Big(\partial_t v_x + v_x \partial_x v_x + \dfrac{1}{r} v_r \partial_r (r v_x)\Big) = -\partial_x p_b + 2\varepsilon^2 \partial_x \Big(\widetilde{G}(\dot\gamma)\, \partial_x v_x\Big) + \dfrac{1}{r}\partial_r \Big(r\, \widetilde{G}(\dot\gamma)\, (\partial_r v_x + \varepsilon^2 \partial_x v_r)\Big) - \partial_x p_{\mathrm{o}}, \\ \varepsilon^3 \mathcal{R}e\Big(\partial_t v_r + v_x \partial_x v_r + \dfrac{1}{r} v_r \partial_r (r v_r)\Big) = -\partial_r p_b + 2\dfrac{\varepsilon^2}{r}\partial_r \Big(r\, \widetilde{G}(\dot\gamma)\, \partial_r v_r\Big) + \varepsilon^2 \partial_x \Big(\widetilde{G}(\dot\gamma)\, (\partial_r v_x + \varepsilon^2 \partial_x v_r)\Big), \\ \partial_x v_x + \dfrac{1}{r}\partial_r (r v_r) = 0, \end{cases}$$

where the dimensionless expression of the shear rate $\dot\gamma$ is given by

$$\dot\gamma = \sqrt{|\partial_x v_x|^2 + |\partial_r v_r|^2 + \Big|\frac{v_r}{r}\Big|^2 + \frac{1}{2}\Big|\frac{1}{\varepsilon}\partial_r v_x + \varepsilon \partial_x v_r\Big|^2}.$$

We note that the function $\widetilde{G}$ appearing in the above equations is related to G by $\widetilde{G}(\dot\gamma) = G\left(\dfrac{P\varepsilon^2}{\mu}\dot\gamma\right)$.

The dimensionless version of Darcy's low governing the flow in the membrane has the following form (see

the subsection 3.1.2 for the dimensional form of these equations):

$$\begin{cases} \varepsilon^2 \partial_x^2 p_m + \dfrac{1}{r}\partial_r(r\partial_r p_m) = 0, \\ u_x = -\dfrac{\mathcal{D}a}{\mathcal{P}_1}\partial_x p_m, \\ u_r = -\dfrac{\mathcal{D}a}{\varepsilon^2\,\mathcal{P}_1}\partial_r p_m, \end{cases}$$

for every $(x, r) \in \omega_m$. Similarly to the blood flow, for every $(x, r) \in \omega_d$ and $t > 0$ the dimensionless dialysate flow is governed by the following system (see the subsection 3.1.3 for the dimensional form of these equations):

$$\begin{cases} \varepsilon \mathcal{R}e\mathcal{P}_1\Big(\partial_t w_x + w_x\partial_x w_x + \dfrac{1}{r}w_r\partial_r(rw_x)\Big) = -\partial_x p_d + \varepsilon^2\mathcal{P}_1\partial_x^2 w_x + \dfrac{\mathcal{P}_1}{r}\partial_r(r\partial_r w_x), \\ \varepsilon^3 \mathcal{R}e\mathcal{P}_1\Big(\partial_t w_r + w_x\partial_x w_r + \dfrac{1}{r}w_r\partial_r(rw_r)\Big) = -\partial_r p_d + \dfrac{\varepsilon^2\mathcal{P}_1}{r}\partial_r(r\partial_r w_r) + \varepsilon^4\mathcal{P}_1\partial_x^2 w_r, \\ \partial_x w_x + \dfrac{1}{r}\partial_r(rw_r) = 0. \end{cases}$$

In order to complete the system, we add the dimensionless versions of the conditions on the interface blood/membrane (see the subsection 3.1.4 for the dimensional form of these equations):

$$\begin{cases} v_r = -\dfrac{\mathcal{D}a}{\varepsilon^2}\partial_r p_m, \\ -\partial_r v_x = B_b v_x, \\ p_m = p_b, \end{cases} \qquad \text{for every } (x, r) \in \gamma_{bm},\ t > 0,$$

and on the interface membrane/dialysate, respectively (see the subsection 3.1.5 for the dimensional form of these equations):

$$\begin{cases} w_r = -\dfrac{\mathcal{D}a}{\varepsilon^2\mathcal{P}_1}\partial_r p_m, \\ \partial_r w_x = B_d w_x, \\ p_m = p_d, \end{cases} \qquad \text{for every } (x, r) \in \gamma_{md},\ t > 0.$$

Finally, we have the following boundary conditions, for every $t > 0$ (see the subsection 3.1.6 for the dimensional form of these equations):

$$\begin{cases} p_b|_{\gamma_{\ell,b}} = 1, & p_b|_{\gamma_{r,b}} = 0, \\ p_d|_{\gamma_{r,d}} = -\mathcal{P}_2, & p_d|_{\gamma_{\ell,d}} = -\mathcal{P}_2 - \mathcal{P}_1, \\ w_r|_{\gamma_d} = w_x|_{\gamma_d} = 0, & \\ \partial_r v_x|_{\gamma_b} = 0, & \end{cases}$$

where $\mathcal{P}_1$ and $\mathcal{P}_2$ are respectively given by (6) and (7).

B Variational formulation

In order to numerical approximate the simplified system obtained in the subsection 3.3, we consider a weak formulation of the system. Since in the previous section we obtained an explicit solution for the pressure p_m inside the membrane (domain ω_m), we write here only the weak formulations in domains ω_b and ω_d.

✓ **Blood flow** (in ω_b):

$$\begin{cases} -\left[\displaystyle\int_0^{\frac{R_1}{R}} r p_b \varphi_1^b \,\mathrm{d}r\right]_{x=0}^{x=1} + \iint_{\omega_b} p_b r \partial_x \varphi_1^b \,\mathrm{d}x\,\mathrm{d}r - \int_{\gamma_{bm}} r\,\widetilde{G}(\dot\gamma)\, B_b v_x \varphi_1^b \,\mathrm{d}x \\ \qquad\qquad - \displaystyle\iint_{\omega_b} r\,\widetilde{G}(\dot\gamma)\,\partial_r v_x \partial_r \varphi_1^b \,\mathrm{d}x\,\mathrm{d}r = \iint_{\omega_b} r \partial_x p_o \varphi_1^b \,\mathrm{d}x\,\mathrm{d}r, \\ \displaystyle\int_{\gamma_{bm}} p_b r \varphi_2^b \,\mathrm{d}x - \iint_{\omega_b} p_b(\varphi_2^b + r\partial_r \varphi_2^b)\,\mathrm{d}x\,\mathrm{d}r = 0, \\ \displaystyle\iint_{\omega_b} \partial_x v_x \varphi_3^b \,\mathrm{d}x\,\mathrm{d}r + \iint_{\omega_b} \frac{1}{r}\partial_r(r v_r)\varphi_3^b \,\mathrm{d}x\,\mathrm{d}r = 0, \end{cases}$$

for every $\varphi_i^b \in V_i^b$ and $i \in \{1,2,3\}$. These variational formulations are standard and V_i^b are Sobolev spaces endowed with the boundary conditions mentioned in Section 3.3. For more details on the variational formulations of equations arriving in modeling of fluid flows see, for instance, the monograph [11].

In order to take into account the boundary condition for v_r on γ_{bm}, it is convenient to make the following change of variable:

$$V_r = v_r + r\widetilde{K}_b(p_d - p_b), \text{ where } \widetilde{K}_b = \frac{\widetilde{\mathcal{D}a} R^2}{R_1^2 \ln(R_2/R_1)}.$$

Using this change of variable, the last equation describing the blood flow becomes

$$\iint_{\omega_b} \partial_x v_x \varphi_3^b \,\mathrm{d}x\,\mathrm{d}r + \iint_{\omega_b} \frac{1}{r}\partial_r(r V_r)\varphi_3^b \,\mathrm{d}x\,\mathrm{d}r - \iint_{\omega_b} 2\widetilde{K}_b(p_d - p_b)\varphi_3^b \,\mathrm{d}x\,\mathrm{d}r = 0,$$

for every $\varphi_3^b \in V_3^b$ and, therefore, V_r verifies $V_r = 0$ on γ_{bm}.

✓ **Dialysate flow** (in ω_d):

$$\begin{cases} -\left[\displaystyle\int_{\frac{R_2}{R}}^1 r p_d \varphi_1^d \,\mathrm{d}r\right]_{x=0}^{x=1} + \iint_{\omega_d} p_d r \partial_x \varphi_1^d \,\mathrm{d}x\,\mathrm{d}r - \int_{\gamma_{md}} \mathcal{P}_1 r \partial_r w_x \varphi_1^d \,\mathrm{d}x - \iint_{\omega_d} \mathcal{P}_1 r \partial_r w_x \partial_r \varphi_1^d \,\mathrm{d}x\,\mathrm{d}r = 0, \\ \left[\displaystyle\int_0^1 p_d r \varphi_2^d \,\mathrm{d}x\right]_{r=\frac{R_2}{R}}^{r=1} - \iint_{\omega_d} p_d(\varphi_2^d + r\partial_r \varphi_2^d)\,\mathrm{d}x\,\mathrm{d}r = 0, \\ \displaystyle\iint_{\omega_d} \partial_x w_x \varphi_3^d \,\mathrm{d}x\,\mathrm{d}r + \iint_{\omega_d} \partial_r \frac{1}{r}(r w_r)\varphi_3^d \,\mathrm{d}x\,\mathrm{d}r = 0, \end{cases}$$

for every $\varphi_i^d \in V_i^d$, where V_i^d are standard Sobolev spaces endowed with the corresponding boundary conditions.

As in the case of the blood flow, in order to take into account the boundary condition for w_r on γ_{md}, the following change of variable is made:

$$W_r = w_r + (1-r)\widetilde{K}_d(p_d - p_b), \text{ where } \widetilde{K}_d = \frac{\widetilde{\mathcal{D}a} R^2}{\mathcal{P}_1 R_2 (R - R_2)\ln(R_2/R_1)}.$$

Therefore, the last equation describing the dialysate flow reads as:

$$\iint_{\omega_d} \partial_x w_x \varphi_3^d \,\mathrm{d}x\,\mathrm{d}r + \iint_{\omega_d} \frac{1}{r}\partial_r(r W_r)\varphi_3^d \,\mathrm{d}x\,\mathrm{d}r - \iint_{\omega_d} \frac{1-2r}{r}\widetilde{K}_d(p_d - p_b)\varphi_3^d \,\mathrm{d}x\,\mathrm{d}r = 0,$$

for every $\varphi_3^d \in V_3^d$. Hence, the new variable W_r satisfies $W_r = 0$ on γ_{md}.

In the remaining part of this appendix we give the variational formulation corresponding to the rescaled system (20) modelling the evolution in time of the concentrations c_i.

✓ **Biochemical concentrations** (in ω):

The system (20) has the following variational formulation: find $c_i \in \mathcal{C}_i$ such that

$$\iint_\omega \partial_t c_i r\varphi_i \,\mathrm{d}x\,\mathrm{d}r + \iint_\omega S_i\left(U_x\partial_x c_i + U_r\partial_r c_i\right) r\varphi_i \,\mathrm{d}x\,\mathrm{d}r + \frac{1}{\mathcal{P}e}\iint_\omega r D_i \partial_r c_i \partial_r \varphi_i \,\mathrm{d}x\,\mathrm{d}r - \frac{\varepsilon^2}{\mathcal{P}e}\int_{\gamma_{r,d}} r D_i \partial_x c_i \varphi_i \,\mathrm{d}r$$
$$+\frac{\varepsilon^2}{\mathcal{P}e}\int_{\gamma_{\ell,b}} r D_i \partial_x c_i \varphi_i \,\mathrm{d}r + \frac{\varepsilon^2}{\mathcal{P}e}\iint_\omega r D_i \partial_x c_i \partial_x \varphi_i \,\mathrm{d}x\,\mathrm{d}r = \frac{1}{\mathcal{F}d}\iint_\omega r F_i(c_1,\ldots,c_5)\varphi_i \,\mathrm{d}x\,\mathrm{d}r,$$

for every $\varphi_i \in \mathcal{C}_i$, where $\mathcal{C}_i$ are Sobolev spaces taking into account the boundary conditions.

C The gradient-type algorithm used for the minimization of the function $\mathcal{J}$.

In this appendix, we explicit an optimization algorithm employed to determine the pressure boundary data from the flow rate data. Given the flow rates $\vec{Q} \in \mathbb{R}^4$ we will minimize the function $\mathcal{J} : \mathbb{R}^4 \longmapsto \mathbb{R}^+$ defined by

$$\mathcal{J}(\vec{P}) = \frac{1}{2}\|\Phi(\vec{P}) - \vec{Q}\|^2,$$

the function Φ mapping a given pressure vector $\vec{P} \in \mathbb{R}^4$ onto the corresponding fluxes vector $\vec{Q} \in \mathbb{R}^4$ (this operation is carried out in the subsection 3.5.1, by directly solving the weak formulation which is well-posed for given pressure data). The gradient-type algorithm that we use is the following

GIVEN $\vec{P}$, ε_1, h, α_0
$\alpha \leftarrow \alpha_0$
WHILE $\left(\ \alpha > \varepsilon_1\ \right)$ DO
  $\vec{S} \leftarrow \displaystyle\sum_{j=1}^{4} \frac{\mathcal{J}(\vec{P} + h\vec{e}_i) - \mathcal{J}(\vec{P})}{h}\vec{e}_i$
  DO
    $\vec{P}^\star \leftarrow \vec{P} - \alpha\,\vec{S}$
    $\alpha \leftarrow \alpha/10$
  UNTIL $\left(\ \mathcal{J}(\vec{P}^\star) \le \mathcal{J}(\vec{P})\ \text{ or }\ \alpha \le \varepsilon_1\ \right)$
  IF $\alpha > \varepsilon_1$ THEN
    $\vec{P} \leftarrow \vec{P}^\star$
    $\alpha \leftarrow \alpha_0$
END

References

[1] Kodwo Annan. Finite volume scheme for double convection-diffusion exchange of solutes in bicarbonate high-flux hollow-fiber dialyzer therapy. *Comput. Math. Methods Med.*, pages Art. ID 973424, 16, 2012.

[2] Kodwo Annan. Mathematical modeling of the dynamic exchange of solutes during bicarbonate dialysis. *Math. Comput. Modelling*, 55(5-6):1691–1704, 2012.

[3] Edith Bauer, Kurt Derfler, Christian Joukhadar, and Wilfred Druml. Citrate kinetics in patients receiving long-term hemodialysis therapy. *American journal of kidney diseases*, 46(5):903–907, 2005.

[4] Silja C. Beck, Sonja Uphoff, Sabine C. Langer, and Manfred Krafczyk. Sensitivity of the slip rate coefficient in fluid flow poroelastic coupling conditions. *PAMM*, 14(1):699–700, 2014.

[5] Carl A Burtis, Edward R Ashwood, and David E Bruns. *Tietz textbook of clinical chemistry and molecular diagnostics*. Elsevier Health Sciences, 2012.

[6] Andrew Davenport. What are the anticoagulation options for intermittent hemodialysis? *Nat Rev Nephrol*, 7(9):499–508, September 2011.

[7] S. Eloot, J. Vierendeels, and P. Verdonck. Optimisation of solute transport in dialysers using a three-dimensional finite volume model. *Computer Methods in Biomechanics and Biomedical Engineering*, 9(6):363–370, 2006. PMID: 17145670.

[8] Sunny Eloot, Dirk De Wachter, Ilse Van Tricht, and Pascal Verdonck. Computational flow modeling in hollow-fiber dialyzers. *Artificial Organs*, 26(7):590–599, 2002.

[9] DTS Falkenhagen and M Brandi. Correlation between activated clotting time and ionized calcium in regular dialysis treatment patients (poster). EDTA, 2011.

[10] Antonio Fasano and Angiolo Farina. Modeling high flux hollow fibers dialyzers. *Discrete Contin. Dyn. Syst. Ser. B*, 17(6):1903–1937, 2012.

[11] Roland Glowinski. Finite element methods for incompressible viscous flow. In *Handbook of numerical analysis, Vol. IX*, Handb. Numer. Anal., IX, pages 3–1176. North-Holland, Amsterdam, 2003.

[12] F. Gotch, P. Kotanko, G. Handelman, and N. Levin. A kinetic model of calcium mass balance during dialysis therapy. *Blood Purif*, 25(1):139–149, 2007.

[13] Kidney Disease: Improving Global Outcomes (KDIGO) CKD-MBD Work Group et al. Kdigo clinical practice guideline for the diagnosis, evaluation, prevention, and treatment of chronic kidney disease-mineral and bone disorder (ckd-mbd). *Kidney international. Supplement*, (113):S1, 2009.

[14] Jin Han, Jun-Fa Xue, Meng Xu, Bao-Song Gui, Li Kuang, and Jian-Ming Ouyang. Coordination dynamics and coordination mechanism of a new type of anticoagulant diethyl citrate with ca2. *Bioinorganic chemistry and applications*, 2013, 2013.

[15] F. Hecht. New development in freefem++. *J. Numer. Math.*, 20(3-4):251–265, 2012.

[16] Jonathan Himmelfarb and T. Alp Ikizler. Hemodialysis. *New England Journal of Medicine*, 363(19):1833–1845, 2010. PMID: 21047227.

[17] Shan Huang, Kerstin Sandholm, Nina Jonsson, Anders Nilsson, Anders Wieslander, Gunilla Grundstrm, Viktoria Hancock, and Kristina N. Ekdahl. Low concentrations of citrate reduce complement and granulocyte activation in vitro in human blood. *Clinical Kidney Journal*, 2014.

[18] Ora Kedem and Aharon Katchalsky. Thermodynamic analysis of the permeability of biological membranes to non-electrolytes. *Biochimica et biophysica Acta*, 27:229–246, 1958.

[19] James P Keener and James Sneyd. *Mathematical physiology*, volume 1. Springer, 1998.

[20] Robert J. Kossmann, Annette Gonzales, Robin Callan, and Suhail Ahmad. Increased efficiency of hemodialysis with citrate dialysate: A prospective controlled study. *Clinical Journal of the American Society of Nephrology*, 4(9):1459–1464, 2009.

[21] Cecile Legallais, Gerardo Catapano, Bodo Von Harten, and Ulrich Baurmeister. A theoretical model to predict the in vitro performance of hemodiafilters. *Journal of Membrane Science*, 168(1):3–15, 2000.

[22] John L Meyer. Formation constants for interaction of citrate with calcium and magnesium lons. *Analytical biochemistry*, 62(1):295–300, 1974.

[23] Manuel Molina Nunez, Rosa de Alarcón, Susana Roca, Gracia Álvarez, MS Ros, Cristina Jimeno, Laura Bucalo, Isabel Villegas, and MA García. Citrate versus acetate-based dialysate in on-line haemodiafiltration. a prospective cross-over study. *Blood purification*, 39(1-3):181–187, 2015.

[24] M Mamun Molla and MC Paul. Les of non-newtonian physiological blood flow in a model of arterial stenosis. *Medical engineering & physics*, 34(8):1079–1087, 2012.

[25] E.V. Musvoto, M.C. Wentzel, R.E. Loewenthal, and G.A. Ekama. Integrated chemicalphysical processes modellingi. development of a kinetic-based model for mixed weak acid/base systems. *Water Research*, 34(6):1857 – 1867, 2000.

[26] Graham Neale and Walter Nader. Practical significance of brinkman's extension of darcy's law: Coupled parallel flows within a channel and a bounding porous medium. *The Canadian Journal of Chemical Engineering*, 52(4):475–478, 1974.

[27] KO Pedersen. Binding of calcium to serum albumin i. stoichiometry and intrinsic association constant at physiological ph, ionic strength, and temperature. *Scandinavian journal of clinical and laboratory investigation*, 28(4):459–469, 1971.

[28] Ana CF Ribeiro, Marisa CF Barros, Ana SN Teles, Artur JM Valente, Victor MM Lobo, Abílio JFN Sobral, and MA Esteso. Diffusion coefficients and electrical conductivities for calcium chloride aqueous solutions at 298.15 k and 310.15 k. *Electrochimica Acta*, 54(2):192–196, 2008.

[29] Herbert B Silber and Julie Rosen. Gadolinium and calcium binding to bovine serum albumin. *Journal of Inorganic and Nuclear Chemistry*, 38(7):1415–1419, 1976.

[30] Marylee Z Southard, Lloyd J Dias, Kenneth J Himmelstein, and Valentino J Stella. Experimental determinations of diffusion coefficients in dilute aqueous solution using the method of hydrodynamic stability. *Pharmaceutical research*, 8(12):1489–1494, 1991.

[31] S. Thijssen, A. Kruse, J. Raimann, V. Bhalani, N.W. Levin, and P. Kotanko. A mathematical model of regional citrate anticoagulation in hemodialysis. *Blood Purif*, 29(2):197–203, 2010.

[32] BS Tilley. Sodium flux during haemodialysis. In *Proceedings of the OCCAM–Fields–MITACS Biomedical Problem Solving Workshop*, 2009.

[33] F Villarroel, E Klein, and F Holland. Solute flux in hemodialysis and hemofiltration membranes. *ASAIO Journal*, 23(1):225–232, 1977.

[34] Rodney R Walters, John F Graham, Robert M Moore, and David J Anderson. Protein diffusion coefficient measurements by laminar flow analysis: method and applications. *Analytical biochemistry*, 140(1):190–195, 1984.

[35] Ken-ichiro Yamamoto, Takehito Ogawa, Masato Matsuda, Akinori Iino, Taiji Yakushiji, Takehiro Miyasaka, and Kiyotaka Sakai. Membrane potential and charge density of hollow-fiber dialysis membranes. *Journal of Membrane Science*, 355(12):182 – 185, 2010.